International Journal of Heat and Mass Transfer 187 (2022) 122572

Contents lists available at ScienceDirect

International Journal of Heat and Mass Transfer

journal homepage: www.elsevier.com/locate/hmt

Theoretical modeling of endovascular drug delivery into a multilayer arterial wall from a drug-coated balloon

Ankur Jain[a,*], Sean McGinty[b,c], Giuseppe Pontrelli[d], Long Zhou[e]

[a] Mechanical and Aerospace Engineering Department, University of Texas at Arlington, Arlington, TX, USA
[b] Division of Biomedical Engineering, University of Glasgow, Glasgow, UK
[c] Glasgow Computational Engineering Centre, University of Glasgow, Glasgow, UK
[d] Istituto per le Applicazioni del Calcolo – CNR Via dei Taurini 19, Rome 00185, Italy
[e] School of Mechanical and Power Engineering, Henan Polytechnic University, Jiaozuo, Henan, China

ARTICLE INFO

Article history:
Received 30 November 2021
Revised 2 January 2022
Accepted 10 January 2022
Available online 5 February 2022

Keywords:
Endovascular drug delivery
Drug-coated balloon
Convection-diffusion-reaction equation
Theoretical modeling

ABSTRACT

Drug-coated balloons (DCBs) are used commonly for delivering drug into diseased arteries. When applied on the inner surface of an artery, drug is transported from the balloon into the multilayer arterial wall through diffusion and advection, where it is ultimately absorbed through binding reactions. Mathematical modeling of these mass transport processes has the potential to help understand and optimize balloon-based drug delivery, thereby ensuring both safety and efficacy. The present work derives a closed-form solution for the multilayer cylindrical convection-diffusion-reaction (CDR) transport problem that occurs in balloon-based endovascular drug delivery. The model is presented for an arbitrary number of layers, and accounts for various transport processes in terms of relevant non-dimensional numbers. Quasi-orthogonality for this multilayer problem is derived. Closed-form expressions for the amounts of drug delivered by the balloon, bound in each arterial layer and lost from the external surfaces are derived. It is shown that only a small fraction of drug from the balloon is actually delivered into the artery during the short exposure time, which is influenced strongly by the diffusion coefficient of the inner-most layer. Further, binding of the drug is found to depend strongly on the reaction coefficient, expressed in terms of the Damköhler number. It is shown that boundary conditions on the inner and outer surfaces, expressed in terms of Sherwood numbers, play a role in drug uptake over a longer time period. The model is general enough to be applicable for a wide variety of scenarios and operational conditions, including an arbitrary number of layers. Results from this work provide fundamental insights into drug transport and uptake processes. In addition, these results may help improve the safety and efficacy of balloon-based drug delivery.

1. Introduction

Coronary angioplasty is a common, minimally invasive procedure used to treat obstructive coronary artery disease (CAD) [1]. Historically, angioplasty consisted of deploying a balloon on the back of a catheter to the site of the obstruction and widening the lumen through inflation of the balloon. Nowadays, the majority of CAD patients will also receive a tiny mesh structure called a drug-eluting stent (DES), in what is known as Percutaneous Coronary Intervention (PCI). The purpose of the stent is to act as a scaffold, allowing blood flow to be maintained in the lumen, while the role of drug elution is to combat the biological response which can lead to excessive neointimal growth and further obstruction to blood flow, a phenomenon known as in-stent restenosis (ISR) [2]. While DES has been successful, there is growing interest in the potential of Drug-Coated Balloon (DCB) technology [3,4], particularly when faced with ISR where a stent has previously been deployed, and increasingly in the context of treating less severe de novo atherosclerotic lesions. While DES have been mathematically and computationally modelled extensively in the literature [5], there is a relative lack of modeling studies related to DCB technology.

DES tends to release drug in a controlled and sustained fashion over a period of weeks to months, which is thought to be broadly consistent with the healing time of the artery following device deployment [5]. However, a DCB typically releases their payload over a matter of seconds or minutes, with around 60 s being representative of current practice. Fig. 1 shows a schematic of balloon deployment inside an artery [1]. It is important to note that the DCB obstructs the artery during delivery - inflating for longer than necessary could therefore have serious consequences for the pa-

* Corresponding author at: 500W First St, Rm 211, Arlington, TX 76019, USA.
E-mail address: jaina@uta.edu (A. Jain).

https://doi.org/10.1016/j.ijheatmasstransfer.2022.122572
0017-9310/

Nomenclature

a	coefficient appearing in velocity term (m^2s^{-1})
b	balloon
c	concentration ($molm^{-3}$)
D	diffusion coefficient (m^2s^{-1})
$\bar{D}$	non-dimensional diffusion coefficient
h	convective mass transfer coefficient (ms^{-1})
k	interfacial mass transfer conductance (ms^{-1})
$\bar{k}$	non-dimensional interfacial mass transfer conductance
M	number of layers
N	eigenfunction norm
Pe	Péclet number
R	radius (m)
r	radial coordinate (m)
Sh	Sherwood number
t	time (s)
β	reaction coefficient (s^{-1})
$\bar{\beta}$	non-dimensional reaction coefficient
γ	non-dimensional interface location
τ	non-dimensional time
ψ	cumulative fraction of drug delivered
χ	cumulative fraction of drug absorbed
ρ	fraction of drug remaining
θ, ϕ	non-dimensional concentrations in Stages A and B, respectively
ξ	non-dimensional radial coordinate
λ	non-dimensional eigenvalue
σ	drug partition coefficient

Subscripts

m	layer number
ref	reference value
0,in	inner (luminal) wall
out	outer (perivascular) wall

tient. This tiny time window for drug delivery makes device design particularly challenging. In other words, one must deliver a sufficient amount of drug rapidly - too much drug may result in toxicity, while too little drug could either be completely ineffective or result in drug action waning before healing is complete. Given the drastically different release kinetics between DCB and DES, it is of interest to mathematically model drug release from a DCB and subsequent distribution within the arterial wall, with a view to extracting insights that may be useful in optimizing their design.

A handful of numerical studies related to DCB are available in the literature [6–11]. Numerical studies are typically computationally expensive and make a number of (different) assumptions to enable solutions to be obtained in a reasonable time frame. Drug delivery from the DCB is typically modeled as either a constant concentration for a finite time [11] or a time-dependent flux [6–10]. All of the aforementioned numerical models assume that drug is transported through the arterial wall due to diffusion. Only two models [8,9] account for advective transport due to the known pressure gradient across the arterial wall. Drug binding is dependent on the physio-chemical properties of the particular drug and is handled in different ways in these models, ranging from linear reversible binding kinetics through to multiple phases of nonlinear reversible binding [12]. While most of these models assume a healthy artery, two of these models account for the presence of a homogeneous atherosclerotic plaque within 3D [11] and 2D [9] geometries: however, the healthy portion of the arterial wall is assumed to be a homogeneous material with the same properties. Only one of these studies incorporates a heterogeneous tissue [8]. A major limitation of each of these numerical models is that they do not consider the multi-layer nature of the arterial wall. Analysis of drug delivery in a multi-layer artery has been reported in a limited number of papers, however, such work either is specific to a two-layer geometry [13,14], neglects curvature of the artery [15] or is completely numerical in nature [16]. Further, most of the literature, both single-layer and multi-layer, addresses stent-based [5,14,15,17], and not balloon-based drug delivery.

While an analytical closed-form solution for the stent drug delivery problem has been presented [17], no such solution exists

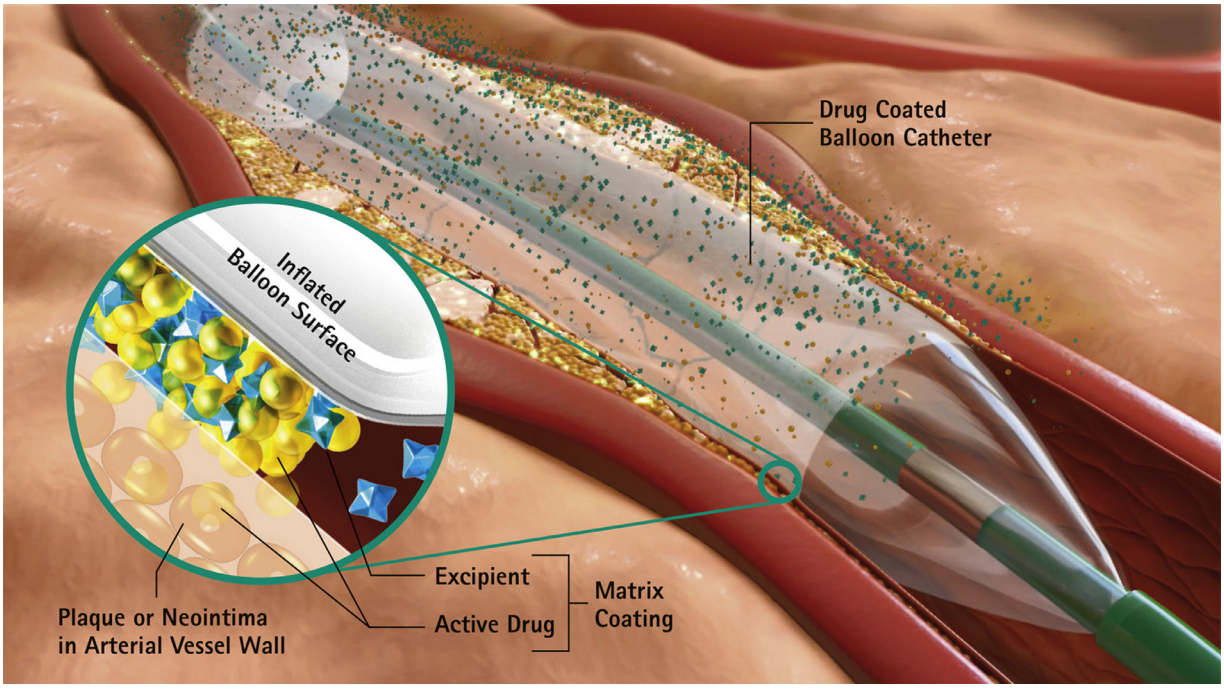

Fig. 1. Picture showing the application of a balloon on the luminal surface of an artery for drug delivery. (Reproduced with permission from [1]).

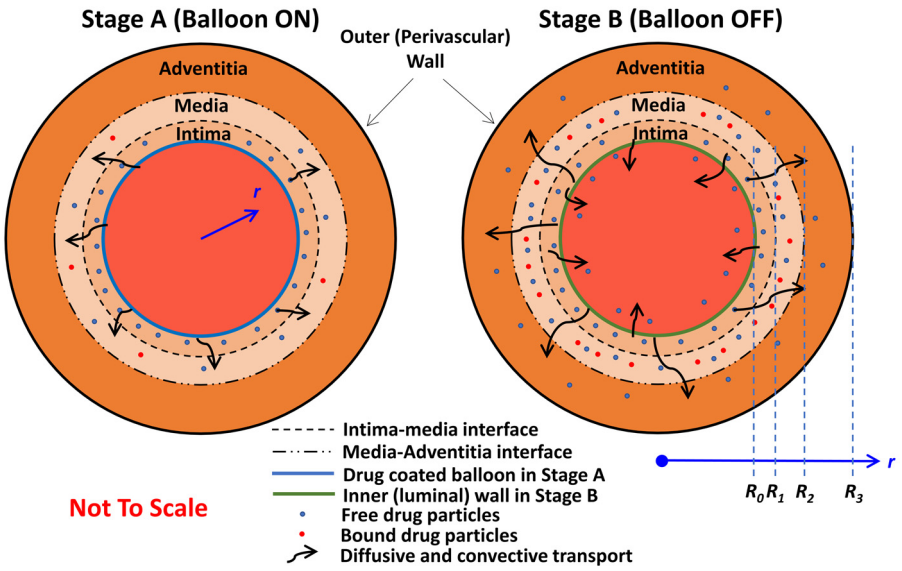

Fig. 2. Schematic of the geometry and boundary conditions for the balloon-driven drug delivery problem for a multi-layer artery. (a) shows Stage A during which the balloon is applied on the luminal surface of the artery, and (b) shows Stage B during which the balloon has been withdrawn.

for the balloon problem, which is fundamentally distinct from the stent problem. Such a solution has the potential to provide key insights into the problem and may allow for rapid evaluation of the influence of various model parameters on key quantities of interest, such as drug delivery into and retention in the tissue. Moreover, analytical solutions may play a key role in providing partial validation for more complex numerical models. While simplifications of the problem are necessary to enable analytical progress, often the key physical processes can be captured with reasonable accuracy.

From a mass transfer perspective, this problem is a multilayer Convection-Diffusion-Reaction (CDR) problem, where, in addition to radial diffusion, transvascular plasma flow causes convection and drug binding in the artery causes reaction. CDR problems have been widely investigated [14,15,18], although only a smaller subset of papers addresses general multilayer CDR problems [18]. Key analytical techniques used for solving such problems include separation of variables [14] and Laplace transformation [19]. In addition, numerical solution of CDR problems has also been carried out [20,21]. It has been shown that multilayer CDR problems may admit imaginary eigenvalues [18], which is why theoretical analysis of such problems is particularly important.

In this paper, a closed-form analytical solution is derived for drug delivery from a DCB and subsequent drug transport and retention in the arterial wall. The model incorporates each of the key physical processes at play, namely drug diffusion, transport through advection and drug binding and retention within a multilayered arterial wall, as shown schematically in Fig. 2. The analytical solution helps understand the impact of various diffusion, convection and binding parameters on the extent of drug delivered by the balloon and bound in the artery as functions of time. Expressions for key safety and efficacy indicators are derived. When compared to similar past work on modeling of endovascular drug delivery, the key novelty of the present work lies in accounting for the multilayer, cylindrical nature of the artery, along with the coupled effects of diffusion, advection and reaction involved in balloon-based drug delivery, all in the context of balloon-based drug delivery. Unlike several past papers, this work is completely analytical, generalized to an arbitrary number of layers and results in closed-form equations for key parameters related to safety and efficacy of drug delivery. Results presented here help understand the fundamentals of the drug delivery process, and may help in the design and optimization of drug carrying balloons towards improved safety and efficacy.

The next section defines, non-dimensionalizes and solves the mass transport problem in a general *M*-layered artery. Section 3 defines and derives expressions for various key safety and efficacy indicators. Results are discussed in detail in Section 4, including expressions for the special case of a homogeneous artery.

2. A general *M*-layer arterial model

2.1. Problem definition

Consider the process of endovascular drug delivery by a drug-coated balloon adhered to the luminal wall of an artery for a short duration, typically 60–120 s in practice [9,11]. During this time, the balloon delivers drug to the luminal wall, from where, drug transport within the arterial layers occurs due to diffusion as well as advection driven by flow of plasma in response to the transmural pressure gradient. Some of the drug is absorbed within the artery due to binding reactions, which are thought to occur predominantly in the media layer where the majority of the target smooth muscle cells reside [16,22]. Finally, the drug may also be lost to the perivascular region from the outer wall. Once the balloon is withdrawn after a short application period, transport and binding processes continue until all the drug has been either bound within the artery or has been lost to the outside medium through the luminal or perivascular wall. It is of interest to develop a mathematical model to predict the drug concentration distribution within the arterial wall as a function of space and time. Specifically, parameters related to safety and efficacy, such as the peak drug distribution in the tissue and the fraction of drug bound in the media layer as a function of time are of interest to device manufacturers and clinicians. Given the short duration of application of the balloon, it is also of interest to determine how much drug is delivered into the artery in that time – such information could help inform drug loading on the balloon. A mathematical model for this balloon-based drug delivery must account for the physical processes described above, as well as the multilayered nature of the artery.

In this work, the generalized case of an M-layered artery is considered first. The special case of a homogeneous artery is then presented in the following section.

Fig. 2 presents a schematic of the geometry, boundary conditions and transport/binding processes in this problem. The multilayer artery is assumed to be sufficiently long relative to its radius and axisymmetric, so that the problem is one-dimensional in the radial direction. A cylindrical coordinate system, with origin at the center axis of the annular cylindrical artery is used, so that the curvature of the artery is accounted for. The artery is modeled as an M-layer annular cylindrical body of inner radius R_0, in which the m^{th} layer is an annular cylinder between $r{=}R_{m\text{-}1}$ and $r{=}R_m$, $m = 1,2..M$. The diffusion coefficient of the drug in the m^{th} layer is given by D_m, assumed to be constant and uniform. Binding reactions in each layer are modeled through first-order reaction kinetics, with a reaction constant of β_m in the m^{th} layer. This assumption is valid when binding is non-saturable and the time scale associated with the unbinding process is much greater than that associated with binding. Existing literature suggests that non-saturable linear binding models may be appropriate for drugs such as heparin [23]. Moreover, for highly lipophilic drugs such as sirolimus, while binding to specific target receptors may be saturable at the typical doses delivered, when non-specific binding is taken into account, total bound drug is likely to be non-saturable at these drug doses [16,22]. In addition, drugs typically coated on DCBs are known to be strongly retained. A flow field $U_m(r)$ driven by transmural pressure difference between the luminal and perivascular regions is also assumed in each layer. In order for the flow field to obey mass conservation, $U_m(r)$ must be inversely proportional to r [17], i.e., $U_m(r){=}a_m/r$. A general convective mass transfer boundary condition, represented by a mass transfer coefficient h_{out} is assumed on the perivascular of the artery, $r{=}r_M$. The value of $h_{out}{=}0$ corresponds to an impermeable wall, whereas h_{out} tending to infinity represents a constant concentration boundary condition at $r{=}r_M$. Drug concentration in the balloon, c_b, is applied to the luminal wall up to time t_b.

Two distinct stages are considered over time, as shown in Fig. 2. In Stage A, $0{<}t{<}t_b$, the balloon is applied on the luminal wall, $r = R_0$, which is modeled by a constant concentration boundary condition based on c_b, the drug concentration in the balloon. In Stage B, $t \geq t_b$, the balloon is removed, so that convective mass transfer to luminal blood flow may also occur at $r = R_0$, which is modeled by a convective mass transfer coefficient h_{in} on the luminal wall.

Based on this problem statement and assumptions, the following governing mass conservation equation for concentration distribution in the m^{th} layer, $c_m(r,t)$ may be written as follows:

$$\frac{\partial c_m}{\partial t} = D_m \frac{1}{r}\frac{\partial}{\partial r}\left(r\frac{\partial c_m}{\partial r}\right) - \frac{a_m}{r}\frac{\partial c_m}{\partial r} - \beta_m c_m \qquad (R_{m-1} < r < R_m)\ (m = 1, 2, 3 \ldots M) \tag{1}$$

which represents a balance between diffusion, convection and reaction terms to determine the evolution of the concentration field over time.

The associated boundary condition on the luminal boundary is

$$\begin{array}{ll} c_1 = c_b & (0 < t < t_b)\ \text{(Stage A)} \\ -D_1\frac{\partial c_1}{\partial r} + \frac{a_1}{r}c_1 + h_{in}c_1 = 0 & (t \geq t_b)\qquad \text{(Stage B)} \end{array} \qquad (at\ r = R_0) \tag{2}$$

On the perivascular surface, one may write

$$D_M\frac{\partial c_M}{\partial r} - \frac{a_M}{r}c_M + h_{out}c_M = 0\ \ (at\ r = R_M) \tag{3}$$

where the outside concentration is taken to be zero for reference.

The following conditions apply at the interfaces

$$-D_m\frac{\partial c_m}{\partial r} + \frac{a_m}{r}c_m = -D_{m+1}\frac{\partial c_{m+1}}{\partial r} + \frac{a_{m+1}}{r}c_{m+1}\ \ (\text{at } r = R_m)\ \ (m = 1, 2 \ldots M-1) \tag{4}$$

$$-D_m\frac{\partial c_m}{\partial r} + \frac{a_m}{r}c_m = k_m(c_m - c_{m+1})\ \ (\text{at } r = R_m)\ \ (m = 1, 2 \ldots M-1) \tag{5}$$

where k_m is the mass transfer conductance at the interface between m^{th} and $(m+1)^{\text{th}}$ layers.

It is assumed that there is no drug present in the artery initially, i.e.,

$$c_m = 0\ \ (at\ t = 0)\ \ (m = 1, 2, 3 \ldots M) \tag{6}$$

Note that the boundary condition at the luminal surface, Eq. (2), changes from a constant concentration condition during Stage A to a convective mass transfer condition during Stage B. The distinct nature of these boundary conditions presents challenges in modeling. For example, while Eq. (2) can be modeled, in principle, with a time-varying step-function h_{in}, which is infinite during Stage A, time-varying convective coefficients are, in general, very difficult to handle, especially in a multilayer geometry [24]. Instead, the problem is solved separately and sequentially, such that the solution at the end of Stage A serves as the initial condition for Stage B. Before this is carried out, however, it is important to non-dimensionalize this problem for ease and generality of analysis.

2.2. Non-dimensionalization

The following non-dimensionalization is carried out:

$$\theta_m = \tfrac{c_m}{c_b}\ \text{(Stage A)},\ \ \phi_m = \tfrac{c_m}{c_b}\ \text{(Stage B)},\ \ \xi = \tfrac{r}{R_M},\ \tau = \tfrac{D_M t}{R_M^2},\ \ \gamma_m = \tfrac{R_m}{R_M},\ \ \gamma_0 = \tfrac{R_0}{R_M},\ \ \bar{D}_m = \tfrac{D_m}{D_M},\ \ \bar{\beta}_m = \tfrac{\beta_m R_M^2}{D_M};$$
$$Pe_m = \tfrac{a_m}{D_M};\ \ \bar{k}_m = \tfrac{k_m R_M}{D_M};\ Sh_{out} = \tfrac{h_{out}\cdot R_M}{D_M};\ \ Sh_{in} = \tfrac{h_{in}\cdot R_M}{D_M};\ \tau_b = \tfrac{D_M t_b}{R_M^2}.$$

Note that Pe_m and $\bar{\beta}_m$ are the Péclet and Damköhler numbers in the m^{th} layer, defined as the ratios of advection and reaction rates, respectively, to the diffusion rate. Sh_{out} is the Sherwood number on the perivascular surface. A very large value of Sh_{out} corresponds to a zero concentration, i.e., infinite sink condition. Sh_{in} is the Sherwood number at the luminal surface, relevant only for Stage B. The Péclet

number here is based on the coefficient a_m instead of the velocity U_m, because the velocity is not a constant, but rather a function of the radial coordinate due to mass conservation in a radial, pressure-driven flow [17].

Based on this non-dimensionalization, the following two sub-sections define and solve the drug concentration problem in Stages A and B.

2.3. Stage A: while balloon is applied ($0 \le \tau \le \tau_b$)

During Stage A, the balloon present on the luminal wall of the artery is modeled as a constant concentration source, as described in the first part of Eq. (2). The following non-dimensional set of governing equations for Stage A may be written as follows:

$$\frac{\partial \theta_m}{\partial \tau} = \frac{\bar{D}_m}{\xi}\frac{\partial}{\partial \xi}\left(\xi \frac{\partial \theta_m}{\partial \xi}\right) - \frac{Pe_m}{\xi}\frac{\partial \theta_m}{\partial \xi} - \bar{\beta}_m \theta_m \ (\gamma_{m-1} < \xi < \gamma_m; 0 < \tau < \tau_b) \ (m = 1, 2, 3 \ldots M) \tag{7}$$

subject to

$$\theta_1 = 1 \ (\text{at } \xi = \gamma_0) \tag{8}$$

$$\frac{\partial \theta_M}{\partial \xi} - \frac{Pe_M \theta_M}{\xi} + Sh_{out}\theta_M = 0 \ (\text{at } \xi = 1) \tag{9}$$

$$-\bar{D}_m \frac{\partial \theta_m}{\partial \xi} + \frac{Pe_m}{\xi}\theta_m = -\bar{D}_{m+1}\frac{\partial \theta_{m+1}}{\partial \xi} + \frac{Pe_{m+1}}{\xi}\theta_{m+1} \ (\text{at } \xi = \gamma_m) \ (m = 1, 2 \ldots M-1) \tag{10}$$

$$-\bar{D}_m \frac{\partial \theta_m}{\partial \xi} + \frac{Pe_m}{\xi}\theta_m = \bar{k}_m(\theta_m - \theta_{m+1}) \ (\text{at } \xi = \gamma_m) \ (m = 1, 2 \ldots M-1) \tag{11}$$

along with the following initial condition:

$$\theta_m = 0 \ (\text{at } \tau = 0) \ (m = 1, 2, ..M) \tag{12}$$

Note that $\tau_b = \frac{D_M t_b}{R_M^2}$ is the non-dimensional time period of application of the balloon. The set of Eqs. (7)–(12) is a multilayer cylindrical CDR problem with the only non-homogeneity present in the boundary condition at $\xi = \gamma_0$. In order to account for this non-homogeneity, one must split the solution as follows:

$$\theta_m(\xi, \tau) = u_m(\xi, \tau) + v_m(\xi) (m = 1, 2, 3 \ldots M) \tag{13}$$

where $v_m(\xi)$ satisfies

$$\frac{\bar{D}_m}{\xi}\left(\xi v_m'\right)' - \frac{Pe_m}{\xi}v_m' - \bar{\beta}_m v_m = 0 \ (\gamma_{m-1} < \xi < \gamma_m) \ (m = 1, 2, 3 \ldots M) \tag{14}$$

along with the boundary and interface conditions

$$v_1 = 1 \text{ at } \xi = \gamma_0 \tag{15}$$

$$v_M' - \frac{Pe_M v_M}{\xi} + Sh_{out} v_M = 0 \text{ at } \xi = 1 \tag{16}$$

$$-\bar{D}_m v_m' + \frac{Pe_m}{\xi}v_m = -\bar{D}_{m+1}v_{m+1}' + \frac{Pe_{m+1}}{\xi}v_{m+1} \text{ at } \xi = \gamma_m \ (m = 1, 2 \ldots M-1) \tag{17}$$

$$-\bar{D}_m v_m' + \frac{Pe_m}{\xi}v_m = \bar{k}_m(v_m - v_{m+1}) \text{ at } \xi = \gamma_m (m = 1, 2 \ldots M-1) \tag{18}$$

A general solution of Eq. (14) may be written as

$$v_m(\xi) = \xi^{\mu_m}[A_{v,m}\mathrm{I}_{\mu_m}(\sigma_m \xi) + B_{v,m}\mathrm{K}_{\mu_m}(\sigma_m \xi)] \tag{19}$$

where I and K are modified Bessel functions of the first and second kind, respectively [25], and $\mu_m = \frac{Pe_m}{2\bar{D}_m}$ is the order of these functions. Further, $\sigma_m = \sqrt{\bar{\beta}_m/\bar{D}_m}$.

Based on the boundary and interface conditions, the following 2 M linear algebraic equations may be written for the 2 M unknowns – $A_{v,m}$ and $B_{v,m}$ (m = 1,2,..M):

$$\gamma_0^{\mu_1}[A_{v,1}\mathrm{I}_{\mu_1}(\sigma_1\gamma_0) + B_{v,1}\mathrm{K}_{\mu_1}(\sigma_1\gamma_0)] = 1 \tag{20}$$

$$\sigma_M\left[A_{v,M}\mathrm{I}_{\mu_M-1}(\sigma_M) - B_{v,M}\mathrm{K}_{\mu_M-1}(\sigma_M)\right] + (Sh_{out} - Pe_M)[A_{v,M}\mathrm{I}_{\mu_M}(\sigma_M) + B_{v,M}\mathrm{K}_{\mu_M}(\sigma_M)] = 0 \tag{21}$$

$$\begin{aligned} &-\bar{D}_m\sigma_m\gamma_m^{\mu_m}\left[A_{v,m}I_{\mu_m-1}(\sigma_m\gamma_m) - B_{v,m}K_{\mu_m-1}(\sigma_m\gamma_m)\right] + \frac{Pe_m}{\gamma_m}\gamma_m^{\mu_m}[A_{v,m}I_{\mu_m}(\sigma_m\gamma_m) + B_{v,m}K_{\mu_m}(\sigma_m\gamma_m)] \\ &= -\bar{D}_{m+1}\sigma_{m+1}\gamma_m^{\mu_{m+1}}\left[A_{v,m+1}I_{\mu_{m+1}-1}(\sigma_{m+1}\gamma_m) - B_{v,m+1}K_{\mu_{m+1}-1}(\sigma_{m+1}\gamma_m)\right] \\ &+\frac{Pe_{m+1}}{\gamma_m}\gamma_m^{\mu_{m+1}}\left[A_{v,m+1}I_{\mu_{m+1}}(\sigma_{m+1}\gamma_m) + B_{v,m+1}K_{\mu_{m+1}}(\sigma_{m+1}\gamma_m)\right] \ (m = 1, 2 \ldots M-1) \end{aligned} \tag{22}$$

$$-\bar{D}_m\sigma_m\gamma_m^{\mu_m}\left[A_{v,m}I_{\mu_m-1}(\sigma_m\gamma_m)-B_{v,m}K_{\mu_m-1}(\sigma_m\gamma_m)\right]+\frac{Pe_m}{\gamma_m}\gamma_m^{\mu_m}[A_{v,m}I_{\mu_m}(\sigma_m\gamma_m)+B_{v,m}K_{\mu_m}(\sigma_m\gamma_m)]$$
$$=\bar{k}_m\left[\gamma_m^{\mu_m}[A_{v,m}I_{\mu_m}(\sigma_m\gamma_m)+B_{v,m}K_{\mu_m}(\sigma_m\gamma_m)]-\gamma_m^{\mu_{m+1}}\left[A_{v,m+1}I_{\mu_{m+1}}(\sigma_{m+1}\gamma_m)+B_{v,m+1}K_{\mu_{m+1}}(\sigma_{m+1}\gamma_m)\right]\right]\ (m=1,2\ldots M-1) \tag{23}$$

Solving Eqs. (20)–(23) through matrix inversion results in $A_{v,m}$ and $B_{v,m}$, and therefore the functions $v_m(\xi)$.

The governing equation and boundary/interface conditions for the remainder of the solution, $u_m(\xi,\tau)$ are given by

$$\frac{\partial u_m}{\partial\tau}=\frac{\bar{D}_m}{\xi}\frac{\partial}{\partial\xi}\left(\xi\frac{\partial u_m}{\partial\xi}\right)-\frac{Pe_m}{\xi}\frac{\partial u_m}{\partial\xi}-\bar{\beta}_m u_m\ (\gamma_{m-1}<\xi<\gamma_m;0<\tau<\tau_b)\ (m=1,2,3\ldots M) \tag{24}$$

subject to

$$u_1=0\ \text{at}\ \xi=\gamma_0 \tag{25}$$

$$\frac{\partial u_M}{\partial\xi}-\frac{Pe_M}{\xi}u_M+Sh_{out}u_M=0\ \text{at}\ \xi=1 \tag{26}$$

$$-\bar{D}_m\frac{\partial u_m}{\partial\xi}+\frac{Pe_m}{\xi}u_m=-\bar{D}_{m+1}\frac{\partial u_{m+1}}{\partial\xi}+\frac{Pe_{m+1}}{\xi}u_{m+1}\ \text{at}\ \xi=\gamma_m\ (m=1,2\ldots M-1) \tag{27}$$

$$-\bar{D}_m\frac{\partial u_m}{\partial\xi}+\frac{Pe_m}{\xi}u_m=\bar{k}_m(u_m-u_{m+1})\ \text{at}\ \xi=\gamma_m\ (m=1,2\ldots M-1) \tag{28}$$

along with the following non-homogeneous initial condition:

$$u_m=-v_m(\xi)\ (\text{at}\ \tau=0)\ (m=1,2,..M) \tag{29}$$

Eqs. (24)–(28) are completely homogeneous, and the only non-homogeneity in the u_m problem appears in the initial condition. Therefore, this multilayer CDR problem may be solved using the technique of separation of variables. Specifically, one may write

$$u_m(\xi,\tau)=\sum_{n=1}^{\infty}\hat{g}_n f_{m,n}(\xi)\exp\left(-\hat{\lambda}_n^2\tau\right)\ (m=1,2,3\ldots M) \tag{30}$$

where $\hat{g}_n$ are coefficients to be determined. By separating out the spatial and time-dependent terms, and substituting $f_{m,n}(\xi)=\xi^{\mu_m}\hat{f}_{m,n}(\xi)$, it can be shown that $\hat{f}_{m,n}(\xi)$ satisfies the Bessel differential equation, and, therefore,

$$f_{m,n}(\xi)=\xi^{\mu_m}\left[\hat{A}_{m,n}\mathrm{J}_{\mu_m}\left(\hat{\omega}_{m,n}\xi\right)+\hat{B}_{m,n}\mathrm{Y}_{\mu_m}\left(\hat{\omega}_{m,n}\xi\right)\right] \tag{31}$$

where, by substituting in the governing energy equation, one may show that

$$\hat{\omega}_{m,n}=\sqrt{\frac{\hat{\lambda}_n^2-\bar{\beta}_m}{\bar{D}_m}}\ (m=1,2\ldots M) \tag{32}$$

$\hat{\lambda}_n$ are the eigenvalues of the problem. $\mathrm{J}_v(x)$ and $\mathrm{Y}_v(x)$ represent Bessel functions of the first and second kind, respectively, and of order v [25].

In order to determine the unknown eigenvalues and coefficients, the transient concentration distribution given by Eq. (30) is inserted into boundary and interface conditions given by Eqs. (25)–(28). This results in

$$\hat{A}_{1,n}\mathrm{J}_{\mu_1}\left(\hat{\omega}_{1,n}\gamma_0\right)+\hat{B}_{1,n}\mathrm{Y}_{\mu_1}\left(\hat{\omega}_{1,n}\gamma_0\right)=0 \tag{33}$$

$$\hat{\omega}_{M,n}\left[\hat{A}_{M,n}\mathrm{J}_{\mu_M-1}\left(\hat{\omega}_{M,n}\right)+\hat{B}_{M,n}\mathrm{Y}_{\mu_M-1}\left(\hat{\omega}_{M,n}\right)\right]=(-Sh_{out}+Pe_M)\left[\hat{A}_{M,n}\mathrm{J}_{\mu_M}\left(\hat{\omega}_{M,n}\right)+\hat{B}_{M,n}\mathrm{Y}_{\mu_M}\left(\hat{\omega}_{M,n}\right)\right] \tag{34}$$

$$\begin{aligned}&-\bar{D}_m\hat{\omega}_{m,n}\gamma_m^{\mu_m}\left(\hat{A}_{m,n}\mathrm{J}_{\mu_m-1}\left(\hat{\omega}_{m,n}\gamma_m\right)+\hat{B}_{m,n}\mathrm{Y}_{\mu_m-1}\left(\hat{\omega}_{m,n}\gamma_m\right)\right)+\frac{Pe_m}{\gamma_m}\gamma_m^{\mu_m}\left[\hat{A}_{m,n}\mathrm{J}_{\mu_m}\left(\hat{\omega}_{m,n}\gamma_m\right)+\hat{B}_{m,n}\mathrm{Y}_{\mu_m}\left(\hat{\omega}_{m,n}\gamma_m\right)\right]\\&=-\bar{D}_{m+1}\hat{\omega}_{m+1,n}\gamma_m^{\mu_{m+1}}\left(\hat{A}_{m+1,n}\mathrm{J}_{\mu_{m+1}-1}\left(\hat{\omega}_{m+1,n}\gamma_m\right)+\hat{B}_{m+1,n}\mathrm{Y}_{\mu_{m+1}-1}\left(\hat{\omega}_{m+1,n}\gamma_m\right)\right)+\\&\frac{Pe_{m+1}}{\gamma_m}\gamma_m^{\mu_{m+1}}\left[\hat{A}_{m+1,n}\mathrm{J}_{\mu_{m+1}}\left(\hat{\omega}_{m+1,n}\gamma_m\right)+\hat{B}_{m+1,n}\mathrm{Y}_{\mu_{m+1}}\left(\hat{\omega}_{m+1,n}\gamma_m\right)\right]\ (m=1,\ldots M-1)\end{aligned} \tag{35}$$

$$\begin{aligned}&-\bar{D}_m\hat{\omega}_{m,n}\gamma_m^{\mu_m}\left(\hat{A}_{m,n}\mathrm{J}_{\mu_m-1}\left(\hat{\omega}_{m,n}\gamma_m\right)+\hat{B}_{m,n}\mathrm{Y}_{\mu_m-1}\left(\hat{\omega}_{m,n}\gamma_m\right)\right)+\frac{Pe_m}{\gamma_m}\gamma_m^{\mu_m}\left[\hat{A}_{m,n}\mathrm{J}_{\mu_m}\left(\hat{\omega}_{m,n}\gamma_m\right)+\hat{B}_{m,n}\mathrm{Y}_{\mu_m}\left(\hat{\omega}_{m,n}\gamma_m\right)\right]\\&=\bar{k}_m\left[\gamma_m^{\mu_m}\left(\hat{A}_{m,n}\mathrm{J}_{\mu_m}\left(\hat{\omega}_{m,n}\gamma_m\right)+\hat{B}_{m,n}\mathrm{Y}_{\mu_m}\left(\hat{\omega}_{m,n}\gamma_m\right)\right)-\gamma_m^{\mu_{m+1}}\left(\hat{A}_{m+1,n}\mathrm{J}_{\mu_{m+1}}\left(\hat{\omega}_{m+1,n}\gamma_m\right)+\hat{B}_{m+1,n}\mathrm{Y}_{\mu_{m+1}}\left(\hat{\omega}_{m+1,n}\gamma_m\right)\right)\right]\ (m=1,\ldots M-1)\end{aligned} \tag{36}$$

Eqs. (33)–(36) represent a set of $2{\cdot}M$ linear homogeneous equations in $2{\cdot}M$ unknowns, $\hat{A}_{m,n}$ and $\hat{B}_{m,n}$ (m = 1,2..M). Due to the homogeneous nature of these equations, a non-trivial solution is admitted only if the determinant of these equations is zero. This requirement constitutes the eigenequation, the roots of which provide the eigenvalues $\hat{\lambda}_n$. An explicit expression for the eigenequation for the general

M-layer case may be derived by carefully manipulating Eqs. (33)–(36), as shown in Supplementary Information. The final eigenequation is

$$\begin{aligned}
&\left[\bar{k}_{M-1}\bar{D}_{M-1}\gamma_{M-1}^{\mu_M}p'_{M-1,n}(\gamma_{M-1})\mathrm{Y}_{\mu_M}\left(\hat{\omega}_{M,n}\gamma_{M-1}\right)\right.\\
&-\bar{k}_{M-1}Pe_{M-1}\gamma_{M-1}^{\mu_M-1}p_{M-1,n}(\gamma_{M-1})\mathrm{J}_{\mu_M}\left(\hat{\omega}_{M,n}\gamma_{M-1}\right)-\bar{k}_{M-1}\bar{D}_M\hat{\omega}_{M,n}\gamma_{M-1}^{\mu_M}p_{M-1,n}(\gamma_{M-1})\mathrm{J}_{\mu_M-1}\left(\hat{\omega}_{M,n}\gamma_{M-1}\right)\\
&-\bar{D}_{M-1}\bar{D}_M\hat{\omega}_{M,n}\gamma_{M-1}^{\mu_M}p'_{M-1,n}(\gamma_{M-1})\mathrm{J}_{\mu_M-1}\left(\hat{\omega}_{M,n}\gamma_{M-1}\right)+\bar{D}_MPe_{M-1}\hat{\omega}_{M,n}\gamma_{M-1}^{\mu_M-1}p_{M-1,n}(\gamma_{M-1})\mathrm{J}_{\mu_M-1}\left(\hat{\omega}_{M,n}\gamma_{M-1}\right)\\
&+\bar{k}_{M-1}Pe_{M-1}\gamma_{M-1}^{\mu_M-1}p_{M-1,n}(\gamma_{M-1})\mathrm{J}_{\mu_M}\left(\hat{\omega}_{M,n}\gamma_{M-1}\right)+\bar{D}_{M-1}Pe_{M-1}\gamma_{M-1}^{\mu_M-1}p'_{M-1,n}(\gamma_{M-1})\mathrm{J}_{\mu_M}\left(\hat{\omega}_{M,n}\gamma_{M-1}\right)\\
&\left.-Pe_{M-1}^2\gamma_{M-1}^{\mu_M-2}p_{M-1,n}(\gamma_{M-1})\mathrm{J}_{\mu_M}\left(\hat{\omega}_{M,n}\gamma_{M-1}\right)\right]/\left[\bar{k}_{M-1}Pe_{M-1}\gamma_{M-1}^{\mu_M-1}p_{M-1,n}(\gamma_{M-1})\mathrm{Y}_{\mu_M}\left(\hat{\omega}_{M,n}\gamma_{M-1}\right)\right.\\
&-\bar{k}_{M-1}\bar{D}_{M-1}\gamma_{M-1}^{\mu_M}p'_{M-1,n}(\gamma_{M-1})\mathrm{Y}_{\mu_M}\left(\hat{\omega}_{M,n}\gamma_{M-1}\right)+\bar{k}_{M-1}\bar{D}_M\hat{\omega}_{M,n}\gamma_{M-1}^{\mu_M}p_{M-1,n}(\gamma_{M-1})\mathrm{Y}_{\mu_M}\left(\hat{\omega}_{M,n}\gamma_{M-1}\right)\\
&-\bar{k}_{M-1}\bar{D}_{M-1}\gamma_{M-1}^{\mu_M}p'_{M-1,n}(\gamma_{M-1})\mathrm{Y}_{\mu_M}\left(\hat{\omega}_{M,n}\gamma_{M-1}\right)+\bar{k}_{M-1}\bar{D}_M\hat{\omega}_{M,n}\gamma_{M-1}^{\mu_M}p_{M-1,n}(\gamma_{M-1})\mathrm{Y}_{\mu_M-1}\left(\hat{\omega}_{M,n}\gamma_{M-1}\right)\\
&+\bar{D}_{M-1}\bar{D}_M\hat{\omega}_{M,n}\gamma_{M-1}^{\mu_M}p'_{M-1,n}(\gamma_{M-1})\mathrm{Y}_{\mu_M-1}\left(\hat{\omega}_{M,n}\gamma_{M-1}\right)-\bar{D}_MPe_{M-1}\hat{\omega}_{M,n}\gamma_{M-1}^{\mu_M-1}p_{M-1,n}(\gamma_{M-1})\mathrm{Y}_{\mu_M-1}\left(\hat{\omega}_{M,n}\gamma_{M-1}\right)\\
&-\bar{k}_{M-1}Pe_{M-1}\gamma_{M-1}^{\mu_M-1}p_{M-1,n}(\gamma_{M-1})\mathrm{Y}_{\mu_M}\left(\hat{\omega}_{M,n}\gamma_{M-1}\right)\\
&\left.-\bar{D}_{M-1}Pe_{M-1}\gamma_{M-1}^{\mu_M-1}p'_{M-1,n}(\gamma_{M-1})\mathrm{Y}_{\mu_M}\left(\hat{\omega}_{M,n}\gamma_{M-1}\right)+Pe_{M-1}^2\gamma_{M-1}^{\mu_M-2}p_{M-1,n}(\gamma_{M-1})\mathrm{Y}_{\mu_M}\left(\hat{\omega}_{M,n}\gamma_{M-1}\right)\right]\\
&\left.+[\hat{\omega}_{M,n}\mathrm{J}_{\mu_M-1}\left(\hat{\omega}_{M,n}\right)-(-Sh_{out}+Pe_M)\mathrm{J}_{\mu_M}\left(\hat{\omega}_{M,n}\right)\right]/\left[\hat{\omega}_{M,n}\mathrm{Y}_{\mu_M-1}\left(\hat{\omega}_{M,n}\right)-(-Sh_{out}+Pe_M)\mathrm{Y}_{\mu_M-1}\left(\hat{\omega}_{M,n}\right)\right]=0
\end{aligned}\tag{37}$$

where the $'$ sign refers to derivative with respect to ξ and the expression for function $p_{M-1,n}(\xi)$ is found in Supplementary Information.

Once the eigenvalues are determined from the roots of this transcendental equation, thereby ensuring that the determinant of the set of Eqs. (33)–(36) is zero, one of the equations in this set is redundant. Further, a general solution for the coefficients $\hat{A}_{m,n}$ and $\hat{B}_{m,n}$ may be obtained by assuming one of the coefficients, say, $\hat{A}_{1,n}$ to be one, and determining all other coefficients in terms of $\hat{A}_{1,n}$ from Eqs. (33)–(35). Explicit expressions for $\hat{A}_{m,n}$ and $\hat{B}_{m,n}$ are presented in Supplementary Information.

Finally, the initial condition and principle of quasi-orthogonality may be used to determine the remaining coefficient $\hat{g}_n$. To do so, Eq. (30) is inserted in the initial conditions given by Eq. (29), resulting in

$$-v_m(\xi)=\sum_{n=1}^{\infty}\hat{g}_n\xi^{\mu_m}\left[\hat{A}_{m,n}\mathrm{J}_{\mu_m}\left(\hat{\omega}_{m,n}\xi\right)+\hat{B}_{m,n}\mathrm{Y}_{\mu_m}\left(\hat{\omega}_{m,n}\xi\right)\right](m=1,2,3\ldots M)\tag{38}$$

The statement of principle of quasi-orthogonality for the cylindrical CDR problem is considerably more complicated than that of a pure-diffusion problem, specifically in terms of the weighing functions associated with each layer. Quasi-orthogonality is proved separately in Appendix A. Based on the results in Appendix A, Eq. (38) is multiplied by $\frac{1}{s_m}[\hat{A}_{m,n'}\mathrm{J}_{\mu m}(\hat{\omega}_{m,n'}\xi)+\hat{B}_{m,n'}\mathrm{Y}_{\mu m}(\hat{\omega}_{m,n'}\xi)]\xi^{1-\mu_m}$, where $\frac{s_{m+1}}{s_m}=\frac{\gamma_m^{1-2\mu_{m+1}}}{\gamma_m^{1-2\mu_m}}$ $(m=1,2..M\text{-}1)$ and $s_1=\gamma_1^{1-2\mu_1}$. The resulting expression is integrated from $\xi=\gamma_m$ to $\xi=\gamma_{m+1}$. The resulting equations are added, which, with the use of principle of quasi-orthogonality given by Eq. (A.5) in Appendix A, leads to

$$\hat{g}_{n'}=\frac{1}{N_{n'}}\sum_{m=1}^{M}\frac{1}{s_m}\int_{\gamma_{m-1}}^{\gamma_m}-v_m(\xi)\left[\hat{A}_{m,n'}\mathrm{J}_{\mu_m}\left(\hat{\omega}_{m,n'}\xi\right)+\hat{B}_{m,n'}\mathrm{Y}_{\mu_m}\left(\hat{\omega}_{m,n'}\xi\right)\right]\xi^{1-\mu_m}d\xi\tag{39}$$

where the norm $N_{n'}$ is given by

$$N_{n'}=\sum_{m=1}^{M}\frac{1}{s_m}\int_{\gamma_{m-1}}^{\gamma_m}\xi\left[\hat{A}_{m,n'}\mathrm{J}_{\mu_m}\left(\hat{\omega}_{m,n'}\xi\right)+\hat{B}_{m,n'}\mathrm{Y}_{\mu_m}\left(\hat{\omega}_{m,n'}\xi\right)\right]^2d\xi\tag{40}$$

This completes the solution for Stage A. During this stage, the drug is expected to enter the multi-layer artery from the luminal wall. Some of the drug may get absorbed within the artery layer and some may be lost from the perivascular wall. The second Stage, in which the balloon has been withdrawn is considered in the next section.

2.4. Stage B: after balloon is withdrawn ($\tau \geq \tau_b$)

Once the balloon has been withdrawn, the drug already present within the artery continues to diffuse, be convected and bind within the artery. The boundary condition at the perivascular wall continues to be characterized by a Sherwood number Sh_{out}, whereas, it is assumed that on the luminal surface, the constant concentration boundary condition due to the balloon is replaced by a general mass transfer boundary condition that models drug loss to the luminal blood flow due to convection. This boundary condition may be characterized by another Sherwood number, $Sh_{in}=\frac{h_{in}R_M}{D_M}$. In this framework, the non-dimensional concentration distribution $\phi_m(\xi,\tau)$ during Stage B is given by

$$\frac{\partial\phi_m}{\partial\tau}=\frac{\bar{D}_m}{\xi}\frac{\partial}{\partial\xi}\left(\xi\frac{\partial\phi_m}{\partial\xi}\right)-\frac{Pe_m}{\xi}\frac{\partial\phi_m}{\partial\xi}-\bar{\beta}_m\phi_m\ (\gamma_{m-1}<\xi<\gamma_m;\ \tau>\tau_b)\ (m=1,2,3\ldots M)\tag{41}$$

subject to

$$-\bar{D}_1\frac{\partial\phi_1}{\partial\xi}+\frac{Pe_1\phi_1}{\xi}+Sh_{in}\phi_1=0\ (\text{at}\ \xi=\gamma_0)\tag{42}$$

$$\frac{\partial\phi_M}{\partial\xi}-\frac{Pe_M\phi_M}{\xi}+Sh_{out}\phi_M=0\ (\text{at}\ \xi=1)\tag{43}$$

$$-\bar{D}_m\frac{\partial\phi_m}{\partial\xi}+\frac{Pe_m}{\xi}\phi_m = -\bar{D}_{m+1}\frac{\partial\phi_{m+1}}{\partial\xi}+\frac{Pe_{m+1}}{\xi}\phi_{m+1}\ (\text{at}\ \ \xi=\gamma_m)\ (m=1,2\ldots M-1) \quad (44)$$

$$-\bar{D}_m\frac{\partial\phi_m}{\partial\xi}+\frac{Pe_m}{\xi}\phi_m = \bar{k}_m(\phi_m-\phi_{m+1})\ (\text{at}\ \xi=\gamma_m)\ (m=1,2\ldots M-1) \quad (45)$$

along with the following initial condition:

$$\phi_m=\theta_m(\xi,\tau_d)\ (\text{at}\ \tau=0)\ (m=1,2,..M) \quad (46)$$

where $\theta_m(\xi,\tau_d)$ is the concentration distribution at the end of Stage A, which serves as the initial condition for Stage B. Note that the time coordinate associated with ϕ_m in these equations begins at the time that the balloon is withdrawn.

This problem is similar to the $u_m(\xi,\tau)$ problem encountered in Stage A. A solution may be written as follows:

$$\phi_m(\xi,\tau)=\sum_{n=1}^{\infty}\tilde{g}_n\xi^{\mu_m}\left[\tilde{A}_{m,n}\mathrm{J}_{\mu_m}(\tilde{\omega}_{m,n}\xi)+\tilde{B}_{m,n}\mathrm{Y}_{\mu_m}(\tilde{\omega}_{m,n}\xi)\right]\times\exp\left(-\tilde{\lambda}_n^2\tau\right)(m=1,2,3\ldots M) \quad (47)$$

where, by substituting in the governing energy equation, one may show that

$$\tilde{\omega}_{m,n}=\sqrt{\frac{\tilde{\lambda}_n^2-\tilde{\beta}_m}{\bar{D}_m}}(m=1,2\ldots M) \quad (48)$$

The coefficients $\tilde{A}_{m,n}$ and $\tilde{B}_{m,n}$ satisfy boundary and interface conditions similar to Eqs. (34)–(36). In addition, due to the change in boundary condition at $\xi=\gamma_0$, the coefficients satisfy the following equation instead of Eq. (33):

$$-\tilde{\omega}_{1,n}\bar{D}_1\left[\tilde{A}_{1,n}\mathrm{J}_{\mu_1-1}(\tilde{\omega}_{1,n}\gamma_0)+\tilde{B}_{1,n}\mathrm{Y}_{\mu_1-1}(\tilde{\omega}_{1,n}\gamma_0)\right]+\left(Sh_{in}+\frac{Pe_1}{\gamma_0}\right)\left[\tilde{A}_{1,n}\mathrm{J}_{\mu_1}(\tilde{\omega}_{1,n}\gamma_0)+\tilde{B}_{1,n}\mathrm{Y}_{\mu_1}(\tilde{\omega}_{1,n}\gamma_0)\right]=0 \quad (49)$$

Similar to the process for $u_m(\xi,\tau)$, the eigenvalues for Stage B may be determined by setting the determinant of equations representing boundary and interface conditions to zero. Subsequently, the coefficients $\tilde{A}_{m,n}$ and $\tilde{B}_{m,n}$ may be determined by first setting $\tilde{A}_{1,n}=1$ and determining the remaining coefficients from these equations. Supplementary Information provides an explicit expression for the eigenequation for Stage B, as well as closed-form recursive expressions for $\tilde{A}_{m,n}$ and $\tilde{B}_{m,n}$.

Finally, the remaining coefficient $\tilde{g}_n$ may be determined by using the initial condition

$$\theta_m(\xi,\tau_d)=\sum_{n=1}^{\infty}\tilde{g}_n\xi^{\mu_m}\left[\tilde{A}_{m,n}\mathrm{J}_{\mu_m}(\tilde{\omega}_{m,n}\xi)+\tilde{B}_{m,n}\mathrm{Y}_{\mu_m}(\tilde{\omega}_{m,n}\xi)\right](m=1,2,3\ldots M) \quad (50)$$

Similar to Stage A, Eq. (50) is multiplied by $\frac{1}{s_m}[\tilde{A}_{m,n'}\mathrm{J}_{\mu_m}(\tilde{\omega}_{m,n'}\xi)+\tilde{B}_{m,n'}\mathrm{Y}_{\mu_m}(\tilde{\omega}_{m,n'}\xi)]\xi^{1-\mu_m}$. The resulting expression is integrated from $\xi=\gamma_m$ to $\xi=\gamma_{m+1}$. The resulting equations are added, which, with the use of principle of quasi-orthogonality as outlined in Appendix A leads to

$$\tilde{g}_{n'}=\frac{1}{\tilde{N}_{n'}}\sum_{m=1}^{M}\frac{1}{s_m}\int_{\gamma_{m-1}}^{\gamma_m}\theta_m(\xi,\tau_d)\left[\tilde{A}_{m,n'}\mathrm{J}_{\mu_m}(\tilde{\omega}_{m,n'}\xi)+\tilde{B}_{m,n'}\mathrm{Y}_{\mu_m}(\tilde{\omega}_{m,n'}\xi)\right]\xi^{1-\mu_m}d\xi \quad (51)$$

where the norm $\tilde{N}_{n'}$ is given by

$$N_{n'}=\sum_{m=1}^{M}\frac{1}{s_m}\int_{\gamma_{m-1}}^{\gamma_m}\xi\left[\tilde{A}_{m,n'}\mathrm{J}_{\mu_m}(\tilde{\omega}_{m,n'}\xi)+\tilde{B}_{m,n'}\mathrm{Y}_{\mu_m}(\tilde{\omega}_{m,n'}\xi)\right]^2d\xi \quad (52)$$

This completes the solution for concentration distribution in Stage B, during which, the drug introduced into the artery in Stage A diffuses and binds further, and some of it may also be lost from the luminal and perivascular surfaces.

3. Key safety and efficacy indicators

Key performance indicators that characterize the safety and efficacy of drug delivery include $\bar{\nu}(\tau)$, the amount of drug delivered up to time τ, $\bar{\chi}_m(\tau)$, the amount of drug bound in the m^{th} layer up to time τ, $\bar{\rho}_m(\tau)$, the amount of drug remaining unbound in the m^{th} layer at time τ, and $\bar{\psi}_{out}(\tau)$ and $\bar{\psi}_{in}(\tau)$, the amounts of drug lost from the perivascular and luminal surfaces, respectively, up to time τ. Note that, by the very definition of the problem, $\bar{\psi}_{in}(\tau)$ is zero during Stage A, when drug is being transported from the balloon into the artery – drug loss from the luminal surface only begins in Stage B when the balloon has been withdrawn. Definitions for these non-dimensional parameters are summarized in Table 1. Closed-form expressions, determined by appropriate integration/differentiation of concentration distributions are given in Appendix B. Note that non-dimensionalization is carried out by dividing the corresponding dimensional quantity by the balloon drug concentration and total artery volume.

It may be noted that by multiplying the governing conservation equations, given by Eq. (1) by ξ, integrating spatially within each layer and over time, and finally adding all equations, one may derive the following overall mass conservation relationship between these quantities:

$$\bar{\nu}(\tau)=\bar{\psi}_{out}(\tau)+\bar{\psi}_{in}(\tau)+\sum_{m=1}^{M}\left[\bar{\chi}_m(\tau)+\bar{\rho}_m(\tau)\right] \quad (53)$$

4. Results and discussion

As shown in Section 2, the general solution for concentration distribution in the multilayer artery depends on several parameters, including thicknesses, diffusion coefficients, velocities and reaction coefficients for each layer and convection coefficients at the boundaries. Values/ranges for these parameters based on past literature [13,15,16,26] are listed in Table 2. A three-layer artery comprising intima, media and adventitia is assumed. Binding reaction is assumed to occur only in the media layer. The intima layer is much thinner and with greater diffusivity than the other two layers. While the nominal value of luminal and perivascular Sherwood numbers is taken to be 1, these may vary in a broad range between 0 and ∞, representing an impenetrable and constant concentration boundary, respectively. For example, following the withdrawal of the balloon, the value of Sh_{in} likely depends on the extent of damage to the inner lining of the arterial wall. Similarly, the value of Sh_{out} depends on the nature of tissue surrounding the artery. Since these values are not fixed, a broad range of values is considered in the analysis presented in this section.

4.1. Convergence of series solution

Since the closed-form analytical solution for concentration distribution derived in Section 2, as well as expressions for various performance parameters derived in Section 3 are all in the form of eigenfunction-based infinite series, it is important to determine the number of terms needed in the series to ensure accuracy. This is an important consideration because such series solutions often

Table 1
Definitions and explicit expressions for various drug delivery and absorption parameters.

	Parameter	Stage A		Stage B	
		Integral definition	Expression	Integral definition	Expression
1	Amount delivered up to time τ	$\bar{\nu}(\tau)=\frac{2\gamma_0}{1-\gamma_0^2}\int_0^{\tau}\left(-\bar{D}_1(\frac{\partial\theta_1}{\partial\xi})_{\xi=\gamma_0}+\frac{Pe_1}{\gamma_0}\right)d\tau^*$	Eq. (B.1) in Appendix B	$\bar{\nu}(\tau)=\frac{-2\gamma_0}{1-\gamma_0^2}\int_0^{\tau_d}\left(-\bar{D}_1(\frac{\partial\theta_1}{\partial\xi})_{\xi=\gamma_0}+\frac{Pe_1}{\gamma_0}\right)d\tau^*$	Eq. (B.6) in Appendix B
2	Amount absorbed in m^{th} layer up to time τ	$\bar{\chi}_m(\tau)=\frac{2\bar{\beta}_m}{1-\gamma_0^2}\int_0^{\tau}\int_{\gamma_{m-1}}^{\gamma_m}\xi\theta_m(\xi,\tau^*)d\xi d\tau^*$	Eq. (B.2) in Appendix B	$\bar{\chi}_m(\tau)=\frac{2\bar{\beta}_m}{1-\gamma_0^2}\left[\int_0^{\tau_d}\int_{\gamma_{m-1}}^{\gamma_m}\xi\theta_m(\xi,\tau^*)d\xi d\tau^*+\int_0^{\tau}\int_{\gamma_{m-1}}^{\gamma_m}\xi\phi_m(\xi,\tau^*)d\xi d\tau^*\right]$	Eq. (B.7) in Appendix B
3	Amount remaining in m^{th} layer at time τ	$\bar{\rho}_m(\tau)=\frac{2}{1-\gamma_0^2}\int_{\gamma_{m-1}}^{\gamma_m}\xi\theta_m(\xi,\tau)d\xi$	Eq. (B.3) in Appendix B	$\bar{\rho}_m(\tau)=\frac{2}{1-\gamma_0^2}\int_{\gamma_{m-1}}^{\gamma_m}\xi\phi_m(\xi,\tau)d\xi$	Eq. (B.8) in Appendix B
4	Amount lost from the perivascular surface up to time τ	$\bar{\psi}_{out}(\tau)=\frac{2Sh_{out}}{1-\gamma_0^2}\int_0^{\tau}\theta_M(1,\tau^*)d\tau^*$	Eq. (B.4) in Appendix B	$\bar{\psi}_{out}(\tau)=\frac{2Sh_{out}}{1-\gamma_0^2}\left[\int_0^{\tau_d}\theta_M(1,\tau^*)d\tau^*+\int_0^{\tau}\phi_M(1,\tau^*)d\tau^*\right]$	Eq. (B.9) in Appendix B
5	Amount lost from luminal surface up to time τ	$\bar{\psi}_{in}(\tau)=0$	Eq. (B.5) in Appendix B	$\bar{\psi}_{in}(\tau)=\frac{2\gamma_0 Sh_{in}}{1-\gamma_0^2}\int_0^{\tau}\phi_1(\gamma_0,\tau^*)d\tau^*$	Eq. (B.10) in Appendix B

Table 2
Values of various problem parameters based on past work [13,15,16,26].

Symbol	Definition	Value	Unit	Source
R_0	Lumen radius	1.5×10^{-3}	m	[16]
h_{in}	Luminal mass transfer coefficient	0 to ∞	ms^{-1}	[13]
h_{out}	Perivascular mass transfer coefficient	0 to ∞	ms^{-1}	[16]
Pe	Péclet number for fluid flow	0–4		[13]
M	Number of arterial layers	3		[15]
$D_1,\ D_2,\ D_3$	Diffusivity in arterial layers	1.67×10^{-11}, 7×10^{-12}, 4×10^{-12}	m^2s^{-1}	[15,16]
$R_1-R_0,\ R_2-R_1,\ R_3-R_2$	Arterial layer thicknesses	10×10^{-6}, 500×10^{-6}, 400×10^{-6}	m	[16]
$k_1,\ k_2$	Interfacial mass transfer conductance	9.6×10^{-6}	ms^{-1}	[16,26]
$\beta_1,\ \beta_2,\ \beta_3$	Reaction coefficient in artery	0, 10^{-4}, 0	s^{-1}	[15]
t_d	Duration of balloon application	60	s	

converge slowly [27], and yet, computing too many terms in the series may lead to unnecessary computational difficulties. Therefore, determining the minimum number of terms needed to be computed is important. In the present problem, since the two key performance parameters are $\bar{\nu}(\tau)$, the total amount of drug delivered up to a given time and $\bar{\chi}_2(\tau)$, the total amount of drug absorbed in the media layer up to a given time, the variation in these quantities with the number of eigenvalues considered is examined. Fig. 3 plots $\bar{\nu}(\tau=\tau_d)$ and $\bar{\chi}_2(\tau=0.017)$ as functions of the number of eigenvalues considered. Fig. 3 shows that $\bar{\chi}_2$ converges very quickly, within around 20 eigenvalues. However, in contrast, $\bar{\nu}$ converges very slowly and takes nearly 1000 eigenvalues to converge. The calculation of such a large number of eigenvalues can be tedious, but in the present case is needed to ensure accuracy. In the present work, eigenvalues are computed by identifying intervals in the eigenfunction plot where the curve crosses the x axis, followed by successive application of Newton-Raphson iterations to accurately determine the root. By automating the process, it is possible to seamlessly compute the eigenvalues for any given set of parameter values. All subsequent plots discussed in this work have been computed using 1000 eigenvalues.

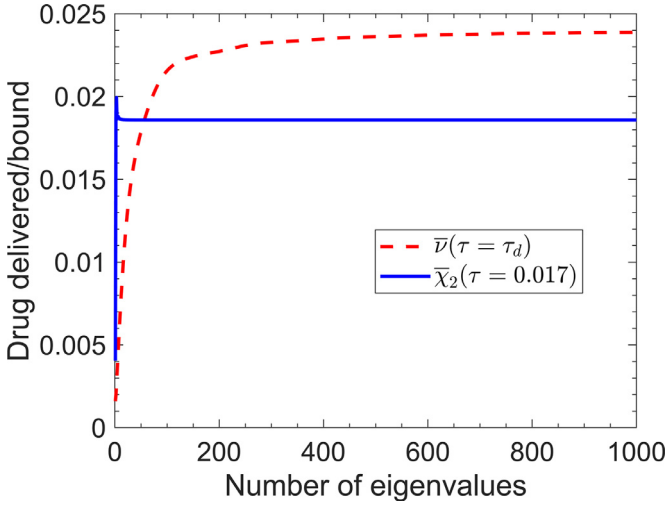

Fig. 3. Effect of number of eigenvalues: Total drug delivered ($\bar{\nu}$) at the end of Stage A and total drug absorbed in media layer ($\bar{\chi}_2$) at $\tau=0.017$ as functions of number of eigenvalues considered.

4.2. Evolution of the concentration field for a representative problem

The concentration field in the three-layer artery in response to drug delivery by a balloon over a small amount of time is computed for a representative set of parameters, as listed in Table 2. The concentration distribution is plotted as a function of ξ at several different times during Stages A and B in Fig. 4(a) and (b), respectively. The intima-media interface location is indicated in both plots.

Note that Stage A is relatively short because the balloon is kept in place only for a short amount of time, so that the non-dimensional duration of Stage A is only $\tau_d=4.1\times10^{-5}$. Fig. 4(a) shows that as time passes, the drug supplied by the balloon at the inner boundary transports farther and farther into the artery. However, the total diffusion length into the artery is relatively short due to the small time period of Stage A. Drug transport clearly crosses over the relatively thin intima and into the media, but does

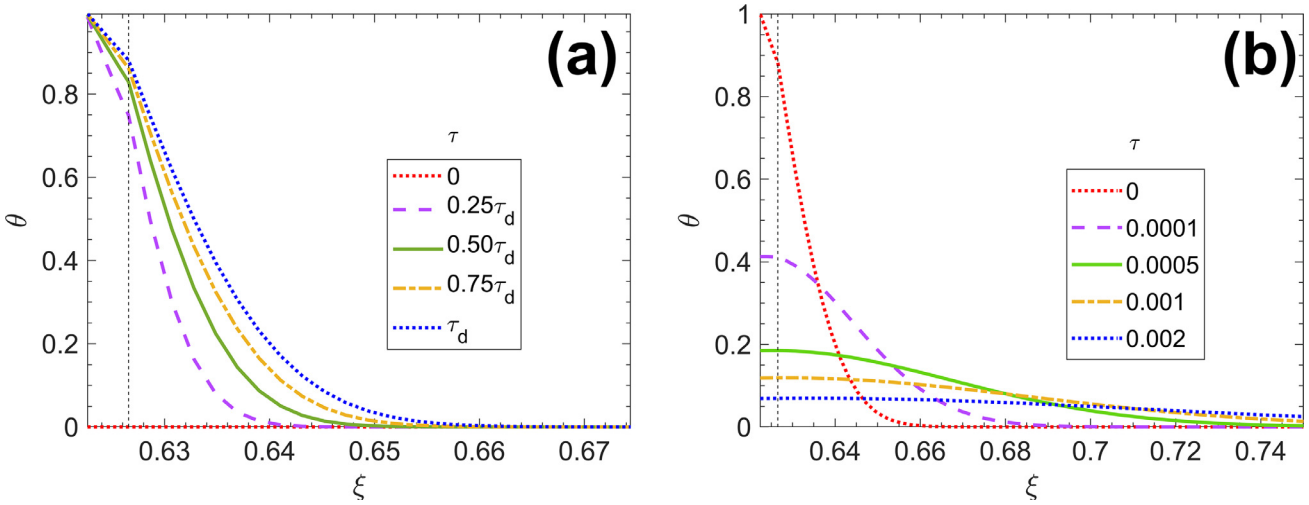

Fig. 4. Plots showing evolution of concentration distribution with time during (a) Stage A; (b) Stage B. Values of other parameters are listed in Table 2. Intima-media interface location is indicated in both plots.

not traverse a large distance into the media layer. The total diffusion length during Stage A shown in Fig. 4(a) is consistent with the diffusion length scale estimate based on diffusivities of the intima and media layers. As a result, the average drug concentration in the media layer at the time of balloon withdrawal is relatively small. The dynamics of drug transport and absorption during Stage B, in which the balloon has been withdrawn, are shown in Fig. 4(b). This plot shows that the drug continues to transport through the artery and be absorbed in the media layer during this Stage. Drug concentration at $\xi = 0$ starts to drop during Stage B, which is because of drug loss at that boundary, at which, the drug-containing balloon has been replaced by a convective boundary condition that represents drug loss to the luminal blood flow. As time passes during Stage B, drug concentration in regions close to the lumen reduces and in regions close to the perivascular region increases due to outwards diffusion and convective transport. Over time, drug loss at the two boundaries as well as drug binding reactions in the media layer all contribute towards a gradual reduction in drug concentration, which, at large times, is either lost from the boundaries or bound within the media layer.

4.3. Overall mass balance during stages A and B

The amount of drug delivered up to any time may be calculated from knowledge of the amount of drug absorbed, still present and lost from the luminal and perivascular surfaces. Section 3 and Table 1 define and present explicit analytical expressions for each of these quantities. It is instructive to examine the evolution of these various quantities over time. Fig. 5(a) and (b) plot these components as functions of time during Stages A and B, respectively. Since drug absorption occurs only in the media layer, $\bar{\chi}_1$ and $\bar{\chi}_3$ are both zero, and therefore are not plotted. Fig. 5(a) shows that during Stage A, when the balloon is present, the amount of drug delivered increases over time. The increase is relatively rapid at early times and slows down later, which is consistent with the nature of diffusion. The amount of drug present in the intima layer rises rapidly due to being next to the drug-containing balloon, before saturating. In contrast, the amount of drug in the media layer rises slowly throughout the time period. Due to the short amount of time in Stage A and the small amount of drug available in the media layer, there is no significant drug absorption in the media layer. The amount of drug lost from the perivascular surface is also approximately zero, which is because not much drug has yet reached the perivascular surface. As shown in Eq. (53), up to any given time, the sum of total drug absorbed and present in all layers, as well as lost from the luminal and perivascular surfaces must add up to the total amount of drug delivered. This total sum is also plotted in Fig. 5(a), and is shown to be very close to the total amount of drug delivered. The overall mass balance shown by this agreement is encouraging and indicates validation of the analysis presented in Section 2.

A similar plot of evolution of drug delivered, absorbed, present and lost during Stage B is presented in Fig. 5(b). As expected, the total amount of drug delivered remains flat during Stage B, because the balloon has been withdrawn, and no more drug enters the artery. Drug present in the three layers of the artery at the start of Stage B continues to transport over time, and can be either absorbed in the media layer, or lost from the luminal and perivascular boundaries. Fig. 5(b) clearly shows that during Stage B, the amount of drug present in intima and media layers reduces as time passes. These layers were saturated with a high drug content during Stage A. In contrast, not much drug transported into the outermost adventitia layer during Stage A, which is why, Fig. 5(b) shows that during Stage B, drug available in the adventitia layer first increases due to diffusion from the media layer, and then gradually decreases due to drug loss at the perivascular surface. The amount of drug lost from the luminal and perivascular surfaces increases and reaches a saturation value. Finally, the amount of drug bound in the media layer rises sharply at first, due to the large amount of drug available in the media layer, and then saturates as the amount of drug available for binding reduces over time. The total amount of drug bound in the media is a small fraction of the drug concentration in the balloon. This indicates that despite the application of the balloon, the amount of drug actually delivered into the media layer is expected to be relatively small compared to drug concentration in the balloon. The drug loading in the balloon must therefore be designed accordingly. Similar to Fig. 5(a), the total sum of drug available, bound and lost is also plotted as a function of time in Fig. 5(b). This sum is found to be close to the total amount of drug delivered, which confirms overall mass balance during Stage B. Note that the time scale over which Stage B has been computed (approximately 3 days) is much longer compared to Stage A (60 s, which is the typical period after which the balloon is withdrawn).

In addition to providing validation of the analytical expressions derived in Section 2, Fig. 5(a) and (b) highlight the interesting dynamics between drug diffusion, advection, absorption and boundary loss. These plots provide practical insights into the design of balloon based drug delivery systems.

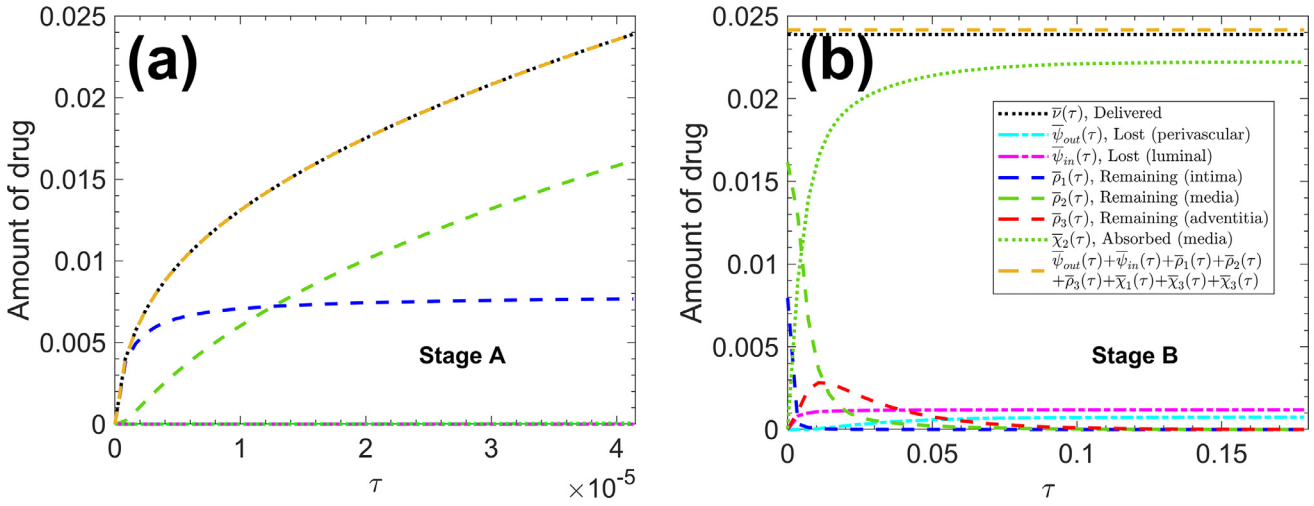

Fig. 5. Overall mass balance plots: amount of drug delivered, lost from the two boundaries, remaining in each of the three layers and absorbed in media layer as functions of time for (a) Stage A, (b) Stage B. Total sum of drug lost, absorbed and remaining is also shown to demonstrate overall mass balance. Values of other parameters are listed in Table 2. For interpretation of curves in (a), please refer to legend in (b).

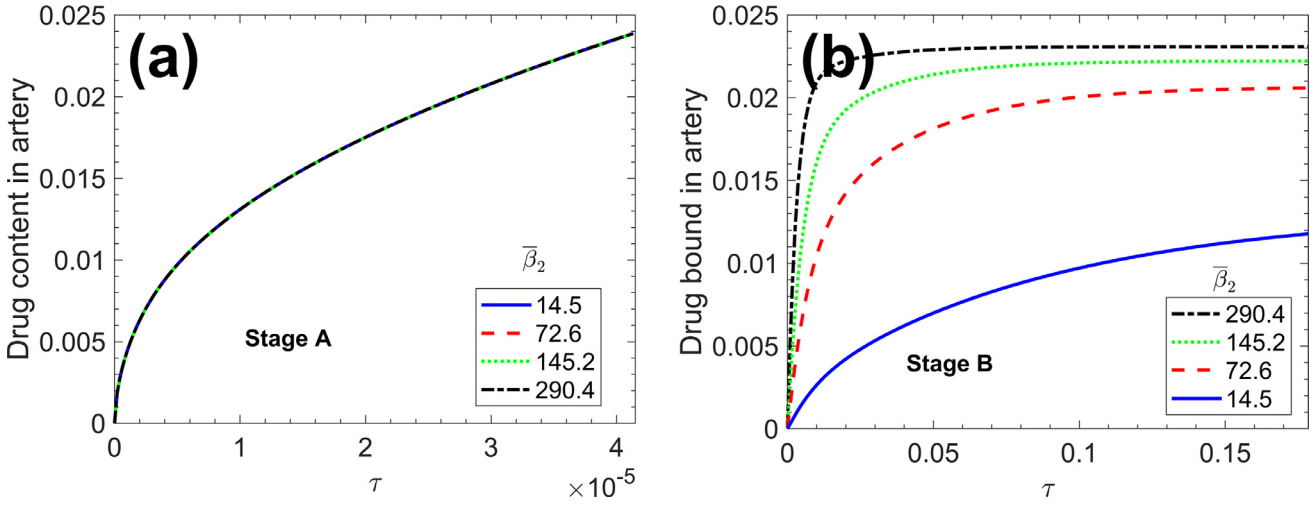

Fig. 6. Effect of reaction coefficient in media layer: (a) drug content in artery as a function of time during Stage A, and (a) drug bound in artery as a function of time during Stage B, both for different values of $\bar{\beta}_2$. Values of other parameters are listed in Table 2.

4.4. Impact of reaction coefficient

The impact of reaction coefficient in the media layer, $\bar{\beta}_2$ on drug content and amount of drug bound in the artery is examined next. Drug content in the artery is the total amount of drug present in all layers of the artery, whether bound or not, and is an important indicator of the safety of the drug delivery process [22]. Fig. 6(a) plots the drug content in the artery as a function of time during Stage A for four different values of $\bar{\beta}_2$, within the range reported in the literature [15]. As expected, there is practically no influence of $\bar{\beta}_2$ on the amount of drug delivered. This is because the amount of drug delivered, and thus contained in the artery mainly depends on the nature of the boundary conditions, as well as diffusion properties of the inner-most arterial layer. This process is largely unrelated to the reaction coefficient in the media layer, especially since only a small amount of drug diffuses into the media layer during the short time period of Stage A.

In contrast, Fig. 6(b) plots the drug bound in the artery as a function of time during Stage B, when most of the drug binding process occurs within the media layer. During this Stage, Fig. 6(b) shows that the larger the value of $\bar{\beta}_2$, the faster is the drug absorption process, and the larger is the amount of drug bound in the artery. This is because a small value of $\bar{\beta}_2$ results in lesser drug binding, and therefore, a greater amount of drug available to diffuse to the boundaries and be lost into the luminal blood flow and surrounding perivascular tissue.

The total drug content in the artery is the sum of bound and unbound drug available in the artery. The impact of the reaction coefficient $\bar{\beta}_2$ on the relative amounts of bound and unbound drug is of interest, and is examined in Supplementary Fig. 1. These two components as well as the total drug content are plotted as functions of $\bar{\beta}_2$ at $\tau = 0.18$. This plots shows that most of the drug is in the bound state: since $\tau = 0.18$ corresponds to a relatively long time, much of the drug delivered by the balloon has been consumed in binding reactions. Supplementary Fig. 1 shows that for very small values of $\bar{\beta}_2$, there may be some unbound drug still remaining at this time.

4.5. Impact of luminal and perivascular boundary conditions

The impact of convective boundary conditions on the luminal and perivascular boundaries, as expressed mathematically by Eqs. (2) and (3) is investigated next. These boundary conditions are represented by Sherwood numbers, Sh_{in} and Sh_{out}, respectively.

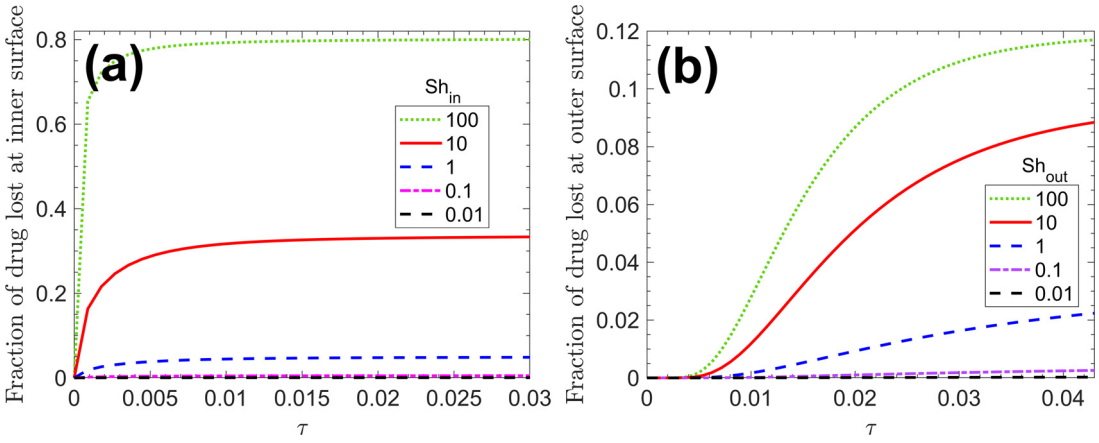

Fig. 7. Impact of luminal and perivascular boundary conditions: Drug lost (as a fraction of total drug delivered) as function of time at (a) luminal surface for different values of Sh_{in}, (b) perivascular surface for different values of Sh_{out}.

The specific value of the Sherwood number depends, among other factors, on the physical properties and functionality of the arterial tissue at these boundaries. For example, application of the balloon on the luminal surface may damage the endothelial cells at that surface, resulting in reduced rate of convective transport at that surface. Further, the nature of tissue surrounding the artery may influence the value of Sh_{out}. Fig. 7(a) and (b) plot the amount of drug lost at the luminal and perivascular surfaces as functions of time for different values of Sh_{in} and Sh_{out}, respectively. The amount of drug lost is expressed as a fraction of the total drug delivered. In both cases, as expected, the greater the Sherwood number, the greater is the amount of drug lost. Note that for a large value of Sh_{in}, up to around 80% of the drug delivered may be lost at the luminal surface. This strong impact is because the luminal surface is close to where most of the drug delivered by the end of Stage A is concentrated. Comparing the dynamics of drug loss at the two surfaces, it is seen that while drug loss at the luminal surface rises sharply with time, drug loss at the perivascular surface lags behind, which is explained by the time taken for the drug to transport through the artery to the perivascular surface. In contrast, drug is readily available close to the luminal surface because that is where the balloon was applied in Stage A. This also explains why the amount of drug lost from the luminal surface is nearly an order of magnitude larger than drug lost from the perivascular surface. Over the time period considered here, the amount of drug lost at the luminal surface reaches a steady value because the drug in the intima layer continues to transport radially outwards and towards the perivascular surface. This is also the reason why drug lost at the perivascular surface takes longer to reach a steady value.

To investigate this further, Fig. 8 plots the amount of drug lost up to a certain time as a function of the Sherwood numbers. Plots for the luminal and perivascular surfaces are presented in Fig. 8(a) and (b), respectively. Similar to Fig. 7, the amount of drug lost is expressed as a fraction of the total drug delivered. As expected, the amount of drug lost increases with increasing value of Sherwood number. A saturation effect is observed in both cases. For example, beyond a value of 100 for Sh_{out}, Fig. 8(b) shows negligible additional drug loss upon increasing Sh_{out} further, indicating that this value is the threshold for reaching an infinite sink boundary condition.

It is also important to examine the impact of the boundary conditions on drug content in the artery. Supplementary Fig. 2 plots drug content in the artery as a function of time during Stage A for different values of the perivascular Sherwood number, Sh_{out}. As expected, Sh_{out} has negligible impact on drug content during Stage A. This is because in the short time duration of Stage A, drug transport into the artery is limited mainly to the intima and media layers, and therefore, the boundary condition on the perivascular surface is relatively insignificant. In contrast, Fig. 9(a) and (b) plot drug content as a function of time in Stage B for different values of luminal and perivascular Sherwood numbers, Sh_{in} and Sh_{out}, respectively. Fig. 9(a) shows a very strong dependence of drug content in the artery on Sh_{in}. For relatively large value of Sh_{in}, the drug content drops dramatically with time. This is because the luminal surface, where Sh_{in} is applied, is located next to the intima, which is rich in drug delivered during Stage A. Therefore, Sh_{in} strongly influences drug content in the artery, and for large values of Sh_{in}, there is significant drug loss from the luminal surface. A large value of Sh_{in} may arise, for example, due to strong convective mass transfer to luminal blood flow, facilitated also by possible endothelial damage due to the application of the balloon. In contrast, the impact of Sh_{out}, which is applied on the perivascular surface, is relatively smaller, particularly in the early part of Stage B, as shown in Fig. 9(b). This is because the perivascular surface is located far from the drug-rich intima, and by the time drug transports to the perivascular surface, so that the impact of Sh_{out} begins to be felt, much of the drug is already bound in the media layer. The five curves shown in Fig. 9(b) are nearly identical at early times, when not much drug has diffused to the perivascular surface, and the influence of Sh_{out} is mainly observed only afterwards.

4.6. Impact of diffusion coefficient of the intima

While each layer in the artery has a distinct diffusion coefficient, that of the intima layer is expected to play a key role in determining the drug delivery and binding characteristics. This is because the intima layer is adjacent to the drug-carrying balloon. Further, drug diffusion during Stage A occurs mainly in the intima layer, and therefore, the total amount of drug delivered before the balloon is withdrawn is strongly dependent on the diffusion coefficient of the intima.

Despite the short duration, Stage A is critical for determining the total amount of drug delivered, because the balloon is withdrawn at the end of Stage A, after which, there is no more drug entering the artery. In order to investigate the impact of intima diffusion coefficient on drug delivery, Fig. 10 plots the amount of drug delivered as a function of time during Stage A for different values of $\bar{D}_1$. The parametric range considered here is one order of magnitude lower and greater than the nominal value based on past

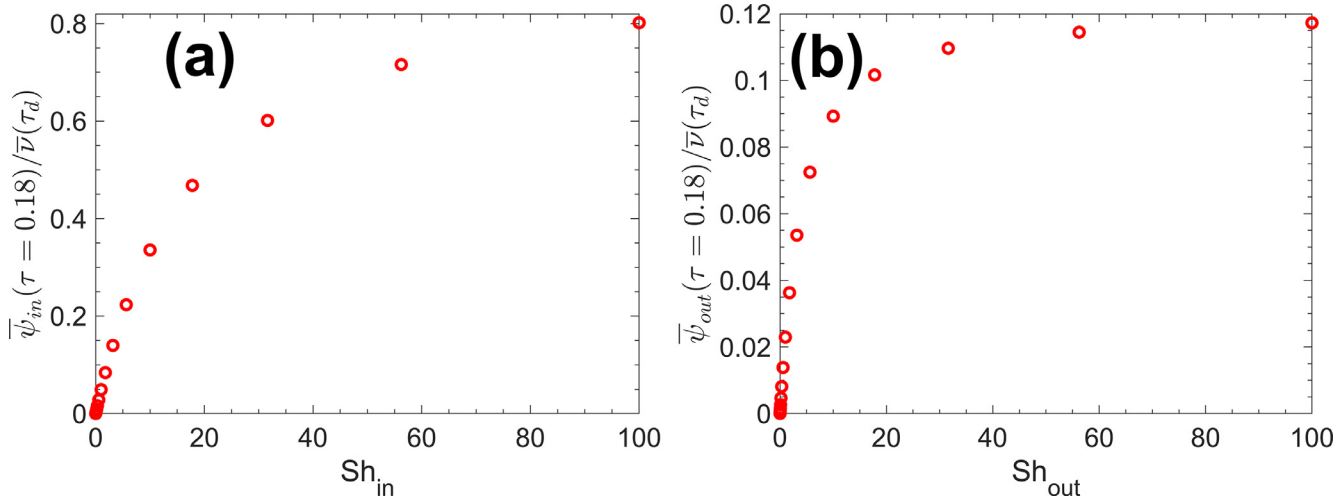

Fig. 8. Impact of luminal and perivascular boundary conditions: drug lost up to $\tau = 0.18$ as a fraction of total drug delivered (a) at luminal surface as a function of Sh_{in}, (a) at perivascular surface as a function of Sh_{out}.

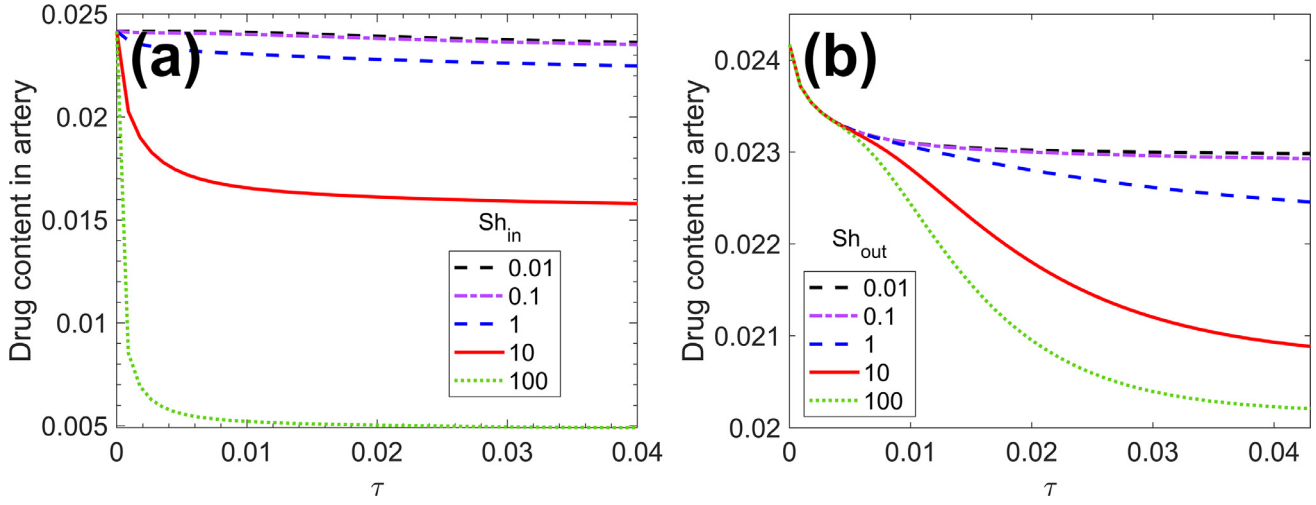

Fig. 9. Effect of luminal and perivascular boundary conditions on drug content: drug content in artery as a function of time for different values of (a) Sh_{in}, (b) Sh_{out}.

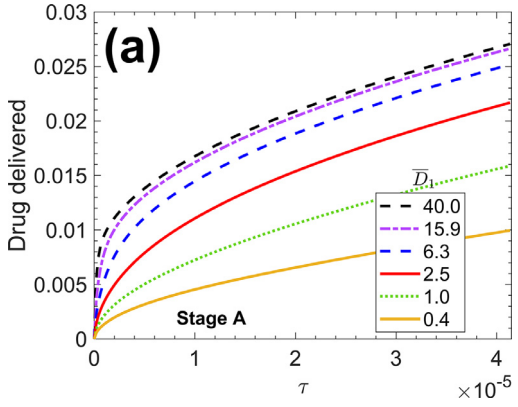

Fig. 10. Effect of intima diffusion coefficient: drug delivered as a function of time during Stage A for different values of $\bar{D}_1$. Values of other parameters are listed in Table 2.

literature [15,16]. Fig. 10 shows that the larger the value of $\bar{D}_1$, the greater is the amount of drug delivered. For each case considered here, the drug delivery curve becomes approximately linear after a short time. However, the greater the value of $\bar{D}_1$, the greater is the initial slope, and thus, the greater is the total amount of drug delivered by the end of Stage A. A saturation effect is also observed, in that once $\bar{D}_1$ is reasonably large, further increase in $\bar{D}_1$ does not significantly increase the amount of drug delivered. This may be because once $\bar{D}_1$ is sufficiently large, drug diffuses very rapidly through the intima, and the overall drug delivery process starts to become limited by $\bar{D}_2$ instead. Note that the intima diffusion coefficient is assumed to not be influenced by the process of applying the balloon on the luminal surface.

Drug content and drug bound in the media is plotted as a function of time for different values of $\bar{D}_1$ in Fig. 11(a) and (b), respectively. During Stage B, the drug content reduces with time due to loss from the boundaries, whereas the amount of drug bound increases with time because of reactions that convert unbound drug available in the media to a bound state. Fig. 11(a) shows very gradual reduction in the drug content over time since the definition of drug content includes both unbound and bound drug. The intima diffusion coefficient only influences the initial drug content at the start of Stage A, and not so much the extent of reduction over time. On the other hand, as shown in Fig. 11(b), the amount of drug bound in the media layer has a strong dependence on $\bar{D}_1$, particularly in the low range of $\bar{D}_1$. This is because the greater the value of $\bar{D}_1$, the more rapid is the rate of diffusion of the drug

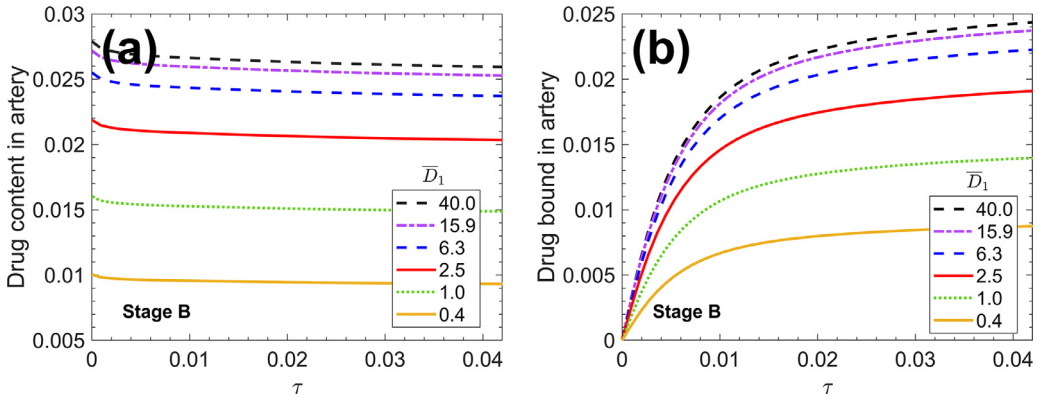

Fig. 11. Effect of intima diffusion coefficient: (a) drug content and (b) drug absorbed as functions of time during Stage B for different values of $\bar{D}_1$. Values of other parameters are listed in Table 2.

from the drug-rich intima into the media, where binding reactions occur. Similar to the effect observed in Fig. 10, there is a saturation effect, in that beyond a threshold value of $\bar{D}_1$, further increase in $\bar{D}_1$ does not result in significant further increase in the amount of drug bound.

4.7. Impact of advection

A key feature of drug transport in this problem is the advection of drug due to radially outwards plasma flow. This radial flow is driven by the transmural pressure difference, and the velocity has been shown to proportional to $1/r$, also depending on the pressure gradient and various porous flow properties [17]. The impact of the Péclet number, which represents the magnitude of this flow field on drug delivery and binding characteristics is examined next. Supplementary Fig. 3(a) and (b) plot the amount of drug delivered during Stage A and amount of drug bound during Stage B as functions of time for several different values of *Pe*, including the baseline value of *Pe*=0 that represents the case of no advection. Note that the range of *Pe* considered is based on estimates derived from existing literature [13]. The plots show that the value of the Péclet number, in the range considered here, has minimal impact on drug delivery and binding characteristics. In Stage B, the amount of drug bound in the media layer actually reduces with increasing Péclet number. This is likely because as *Pe* increases, a greater amount of drug is removed from the media layer and into the adventitia due to advection than is brought into the media from the intima. Note that there are several second-order effects that are not considered in this analysis. For example, the application of the balloon is likely to increase the transmural pressure gradient during Stage A. Due to the relatively short time duration of Stage A, it is anticipated that the effect on the performance indicators considered in this model will be small and, therefore, a constant Péclet number is assumed throughout the time duration considered here. Further, the application of the balloon may damage endothelial cells in the intima layer, which may impact the nature of porous flow through the intima, and therefore, the Péclet number. However, the intima thickness is only 5% of the overall artery thickness, and therefore, this is also likely to be a small effect.

4.8. Results for a homogeneous artery

In some cases, it may be acceptable to neglect the multi-layer nature of the artery, and instead treat it as a homogeneous body. The drug transport problem can be considerably simplified in such a case. Due to the practical importance of this special case, it is instructive to explicitly write the solution for this problem. The governing equations and solution for this problem can be derived by setting $M = 1$ in Section 2. These equations and closed-form expressions for concentration distribution and various performance indicators for this case are summarized in Supplementary Information.

5. Summary and conclusions

Endovascular drug delivery involves complex interactions between several physical and biological processes, including diffusion, advection and binding reactions, which is further complicated by the multilayer nature of the artery. Experimental investigation of drug delivery is time-consuming, expensive and may raise ethical questions where animals are used, which is why mathematical models can provide valuable insights and guidance into appropriate design of experiments. The general mathematical model presented in this work may fulfill this role for arterial drug delivery from a balloon. Key insights gained from this work include the important role of intima diffusion coefficient and media reaction rate in determining the amount of drug delivered and bound, respectively. The model also highlights the key role played by the nature of boundary conditions in this process. Such insights can be used to balance safety and efficacy.

It is important to re-emphasize the key assumptions made here, necessarily employed to enable a closed-form analytical solution. Only one linear, non-saturable binding reaction is assumed to occur. Boundary conditions, as well as transvascular pressure, which influences the Péclet number, are assumed to not be influenced by balloon application or withdrawal. All properties are assumed to be uniform and independent of concentration. For a broad range of practical scenarios, these assumptions are reasonable. Further, note that while values of various properties were taken from existing literature, an integrated effort to measure these properties in the same arterial system, and to study possible variations in these values, may help further improve the accuracy of model predictions.

In addition to the practical insights into the endovascular drug delivery problem, this work also contributes towards theoretical heat and mass transfer by presenting an analytical solution for the multilayer cylindrical CDR problem, including the nature of quasi-orthogonality.

Declaration of Competing Interest

None.

CRediT authorship contribution statement

Ankur Jain: Conceptualization, Methodology, Formal analysis, Validation, Investigation, Data curation, Supervision, Project administration, Writing – original draft, Writing – review & editing. **Sean McGinty:** Conceptualization, Methodology, Formal analysis, Validation, Writing – original draft, Writing – review & editing. **Giuseppe Pontrelli:** Conceptualization, Methodology, Formal analysis, Validation, Writing – original draft, Writing – review & editing. **Long Zhou:** Methodology, Validation, Data curation, Writing – original draft, Writing – review & editing.

Acknowledgments

Funding from the European Research Council under the European Union Horizon 2020 Framework Programme (No. FP/2014-2020) ERC Grant Agreement No. 739964 (COPMAT) is acknowledged. This work is also partially supported by Italian MIUR (PRIN 2017 project: Mathematics of active materials: from mechanobiology to smart devices, project number 2017KL4EF3) .

Appendix A: quasi-orthogonality of eigenfunctions for the general *M*-layer cylinder case with diffusion, convection and reaction

For pure-diffusion multilayer problems, quasi-orthogonality of eigenequations is well-known, and has been widely used for solving standard problems. In the present problem, however, due to the presence of advection and reaction terms in addition to diffusion, the quasi-orthogonality relationship between eigenfunctions is not obvious. This Appendix derives an orthogonality relationship that accounts for these transport processes.

For the general *M*-layer cylindrical geometry considered in this work, the spatial component of the solution, $f_{m,n}$ for the m^{th} layer is given by Eq. (31). For two distinct numbers n and j, $f_{m,n}$ and $f_{m,j}$ satisfy

$$f''_{m,n}+\left(1-\frac{Pe_m}{\bar{D}_m}\right)\frac{f'_{m,n}}{\xi}+\frac{\left(\lambda_n^2-\bar{\beta}_m\right)}{\bar{D}_m}f_{m,n}=0 \tag{A.1}$$

$$f''_{m,j}+\left(1-\frac{Pe_m}{\bar{D}_m}\right)\frac{f'_{m,j}}{\xi}+\frac{\left(\lambda_j^2-\bar{\beta}_m\right)}{\bar{D}_m}f_{m,j}=0 \tag{A.2}$$

For each m, multiply Eqs. (A.1) and (A.2) by $f_{m,j}\xi^{1-2\mu_m}$ and $f_{m,n}\xi^{1-2\mu_m}$, respectively, then subtract to obtain

$$\left[\left(f'_{m,n}f_{m,j}-f'_{m,j}f_{m,n}\right)\xi^{1-2\mu_m}\right]'=-\frac{\left(\lambda_n^2-\lambda_j^2\right)}{\bar{D}_m}f_{m,n}f_{m,j}\xi^{1-2\mu_m} \tag{A.3}$$

Now, for each layer, m, Eq. (A.3) is divided by u_m, where $\frac{u_{m+1}}{u_m}=\frac{{\gamma_m}^{1-2\mu_{m+1}}}{{\gamma_m}^{1-2\mu_m}}$ (m = 1,2,..*M*-1) and $u_1={\gamma_1}^{1-2\mu_1}$. Each of the resulting equations is integrated within the respective layer, and added, to result in

$$\begin{aligned}&-\bar{D}_1\frac{\left[f'_{1,n}(\gamma_0)f_{1,j}(\gamma_0)-f'_{1,j}(\gamma_0)f_{1,n}(\gamma_0)\right]}{{\gamma_1}^{1-2\mu_1}}+\frac{\left[f'_{M,n}(1)f_{M,j}(1)-f'_{M,j}(1)f_{M,n}(1)\right]}{{\gamma_{M-1}}^{1-2\mu_M}}\\&+\sum_{m=2}^{M}\left[\bar{D}_{m-1}\left(f'_{m-1,n}(\gamma_{m-1})f_{m-1,j}(\gamma_{m-1})-f'_{m-1,j}(\gamma_{m-1})f_{m-1,n}(\gamma_{m-1})\right)-\bar{D}_m\left(f'_{m,n}(\gamma_{m-1})f_{m,j}(\gamma_{m-1})-f'_{m,j}(\gamma_{m-1})f_{m,n}(\gamma_{m-1})\right)\right]\\&=\left(\lambda_n^2-\lambda_j^2\right)\sum_{(m=1)}^{M}\frac{1}{u_m}\int_{\gamma_{m-1}}^{\gamma_m}f_{m,n}f_{m,j}\xi^{1-2\mu_m}d\xi\end{aligned} \tag{A.4}$$

The first term on the left hand side of Eq. (A.4) is zero because from the boundary condition at $\xi=\gamma_0$ during Stage A, $f_{1,n}(\gamma_0)=f_{1,j}(\gamma_0)=0$. Similarly, the second term in the left-hand side of Eq. (A.4) may be shown to be zero, based on the boundary condition at $\xi=1$.

Focusing on the remaining terms on the left hand side, each term within the square bracket inside the summation pertains to the interface between the $(m\text{-}1)^{\text{th}}$ and m^{th} layer (m = 2,..*M*). Each term in this summation can be shown to be zero as follows: From the interface condition at $\xi=\gamma_{m-1}$ given by Eq. (10), $\bar{D}_{m-1}f'_{m-1,n}=\bar{D}_m f'_{m,n}-\frac{Pe_m}{\gamma_{m-1}}f_{m,n}+\frac{Pe_{m-1}}{\gamma_{m-1}}f_{m-1,n}$ and $\bar{D}_{m-1}f'_{m-1,j}=\bar{D}_m f'_{m,j}-\frac{Pe_m}{\gamma_{m-1}}f_{m,j}+\frac{Pe_{m-1}}{\gamma_{m-1}}f_{m-1,j}$. Further, from Eq. (11), $\bar{D}_{m-1}f'_{m-1,n}=\frac{Pe_{m-1}}{\gamma_{m-1}}f_{m-1,n}-\bar{k}_{m-1}(f_{m,n}-f_{m-1,n})$ and $\bar{D}_{m-1}f'_{m-1,j}=\frac{Pe_{m-1}}{\gamma_{m-1}}f_{m-1,j}-\bar{k}_{m-1}(f_{m,j}-f_{m-1,j})$. Here, all functions are evaluated at $\xi=\gamma_{m-1}$. Using these relationships, each term within square bracket inside the summation on the left hand side of Eq. (A.4) can be re-arranged as $\frac{Pe_{m-1}}{\gamma_{m-1}}f_{m-1,j}f_{m-1,n}-\bar{k}_{m-1}(f_{m,n}-f_{m-1,n})f_{m-1,j}-\frac{Pe_{m-1}}{\gamma_{m-1}}f_{m-1,j}f_{m-1,n}+\bar{k}_{m-1}(f_{m,n}-f_{m-1,j})f_{m-1,n}-(f'_{m,n}f_{m,j}-f'_{m,j}f_{m,n})$, which can be further simplified to $\bar{k}_{m-1}(f_{m,j}f_{m-1,n}-f_{m,n}f_{m-1,j})-(\frac{Pe_m}{\gamma_{m-1}}f_{m,n}f_{m,j}-\bar{k}_{m-1}(f_{m,n}-f_{m-1,n})f_{m,j}-\frac{Pe_m}{\gamma_{m-1}}f_{m,j}f_{m,n}-\bar{k}_{m-1}(f_{m,j}-f_{m-1,j})f_{m,n})$, which is zero.

This shows that the left hand side of Eq. (A.4) is zero. Therefore, for distinct n and j, the following relationship between the spatial eigenfunctions may be written:

$$\sum_{m=1}^{M}\frac{1}{u_m}\int_{\gamma_{m-1}}^{\gamma_m}f_{m,n}f_{m,j}\xi^{1-2\mu_m}d\xi=0\quad n\neq j \tag{A.5}$$

This orthogonality relationship differs from the standard orthogonality for pure-diffusion multilayer problems in the $\xi^{1-2\mu_m}$ term as well as the definition of u_m. Eq. (A.5) plays an important role in deriving an expression for the last remaining coefficient, $\hat{g}_n$ of the problem.

Along similar lines, it can be shown that the orthogonality relationship given by Eq. (A.5) also holds for the eigenfunctions for Stage B.

Appendix B: explicit expressions for parameters

By inserting Eqs. (13) and (47) in the definitions for various performance parameters given in Table 1, one may derive the following explicit expressions:

Stage A:

$$\bar{\nu}(\tau)=\frac{-2\gamma_0}{1-\gamma_0^2}\times \left[\left[A_{\nu,1}I_{\mu_1-1}(\sigma_1\gamma_0)-B_{\nu,1}K_{\mu_1-1}(\sigma_1\gamma_0)\right]\sigma_1\gamma_0^{\mu_1}\tau+\sum_{n=1}^{\infty}\hat{g}_n\left(\hat{A}_{1,n}J_{\mu_1-1}\left(\hat{\omega}_{1,n}\gamma_0\right)+\hat{B}_{1,n}Y_{\mu_1-1}\left(\hat{\omega}_{1,n}\gamma_0\right)\right)\hat{\omega}_{1,n}\gamma_0^{\mu_1}\left(\frac{1-\exp\left(-\hat{\lambda}_n^2\tau\right)}{\hat{\lambda}_n^2}\right)\right] \tag{B.1}$$

$$\begin{aligned}\bar{\chi}_m(\tau)=&\frac{2\tilde{\beta}_m}{1-\gamma_0^2}\times\\ &\left[\left[A_{\nu,m}I_{\mu_m+1}(\sigma_m\gamma_m)-B_{\nu,m}K_{\mu_m+1}(\sigma_m\gamma_m)\right]\frac{\gamma_m^{\mu_m+1}}{\sigma_m}\tau-\right.\\ &\left[A_{\nu,m}I_{\mu_m+1}(\sigma_m\gamma_{m-1})-B_{\nu,m}K_{\mu_m+1}(\sigma_m\gamma_{m-1})\right]\frac{\gamma_{m-1}^{\mu_m+1}}{\sigma_m}\tau\\ &+\sum_{n=1}^{\infty}\frac{\hat{g}_n}{\hat{\omega}_{m,n}}\left[\left(\hat{A}_{m,n}J_{\mu_m+1}\left(\hat{\omega}_{m,n}\gamma_m\right)+\hat{B}_{m,n}Y_{\mu_m+1}\left(\hat{\omega}_{m,n}\gamma_m\right)\right)\gamma_m^{\mu_m+1}-\left(\hat{A}_{m,n}J_{\mu_m+1}\left(\hat{\omega}_{m,n}\gamma_{m-1}\right)+\hat{B}_{m,n}Y_{\mu_m+1}\left(\hat{\omega}_{m,n}\gamma_{m-1}\right)\right)\gamma_{m-1}^{\mu_m+1}\right]\left(\frac{1-\exp\left(-\hat{\lambda}_n^2\tau\right)}{\hat{\lambda}_n^2}\right)\Bigg]\end{aligned} \tag{B.2}$$

$$\begin{aligned}\bar{\rho}_m(\tau)=&\frac{2}{1-\gamma_0^2}\times\\ &\left[\left[A_{\nu,m}I_{\mu_m+1}(\sigma_m\gamma_m)-B_{\nu,m}K_{\mu_m+1}(\sigma_m\gamma_m)\right]\frac{\gamma_m^{\mu_m+1}}{\sigma_m}-\left[A_{\nu,m}I_{\mu_m+1}(\sigma_m\gamma_{m-1})-B_{\nu,m}K_{\mu_m+1}(\sigma_m\gamma_{m-1})\right]\frac{\gamma_{m-1}^{\mu_m+1}}{\sigma_m}+\right.\\ &\left.\sum_{n=1}^{\infty}\frac{\hat{g}_n}{\hat{\omega}_{m,n}}\left[\left(\hat{A}_{m,n}J_{\mu_m+1}\left(\hat{\omega}_{m,n}\gamma_m\right)+\hat{B}_{m,n}Y_{\mu_m+1}\left(\hat{\omega}_{m,n}\gamma_m\right)\right)\gamma_m^{\mu_m+1}-\left(\hat{A}_{m,n}J_{\mu_m+1}\left(\hat{\omega}_{m,n}\gamma_{m-1}\right)+\hat{B}_{m,n}Y_{\mu_m+1}\left(\hat{\omega}_{m,n}\gamma_{m-1}\right)\right)\gamma_{m-1}^{\mu_m+1}\right]\exp\left(-\hat{\lambda}_n^2\tau\right)\right]\end{aligned} \tag{B.3}$$

$$\bar{\psi}_{out}(\tau)=\frac{2Sh_{out}}{1-\gamma_0^2}\times \left[\left[A_{\nu,M}I_{\mu_M}(\sigma_M)+B_{\nu,M}K_{\mu_M}(\sigma_M)\right]\tau+\sum_{n=1}^{\infty}\hat{g}_n\left[\hat{A}_{M,n}J_{\mu_M}\left(\hat{\omega}_{M,n}\right)+\hat{B}_{M,n}Y_{\mu_M}\left(\hat{\omega}_{M,n}\right)\right]\left(\frac{1-\exp\left(-\hat{\lambda}_n^2\tau\right)}{\hat{\lambda}_n^2}\right)\right] \tag{B.4}$$

$$\bar{\psi}_{in}(\tau)=0 \tag{B.5}$$

Stage B:

$$\bar{\nu}(\tau)=\frac{-2\gamma_0}{1-\gamma_0^2}\times \left[\left[A_{\nu,1}I_{\mu_1-1}(\sigma_1\gamma_0)-B_{\nu,1}K_{\mu_1-1}(\sigma_1\gamma_0)\right]\sigma_1\gamma_0^{\mu_1}\tau_d+\sum_{n=1}^{\infty}\hat{g}_n\left(\hat{A}_{1,n}J_{\mu_1-1}\left(\hat{\omega}_{1,n}\gamma_0\right)+\hat{B}_{1,n}Y_{\mu_1-1}\left(\hat{\omega}_{1,n}\gamma_0\right)\right)\hat{\omega}_{1,n}\gamma_0^{\mu_1}\left(\frac{1-\exp\left(-\hat{\lambda}_n^2\tau_d\right)}{\hat{\lambda}_n^2}\right)\right] \tag{B.6}$$

$$\begin{aligned}\bar{\chi}_m(\tau)=&\frac{2\tilde{\beta}_m}{1-\gamma_0^2}\left[\left[A_{\nu,m}I_{\mu_m+1}(\sigma_m\gamma_m)-B_{\nu,m}K_{\mu_m+1}(\sigma_m\gamma_m)\right]\frac{\gamma_m^{\mu_m+1}}{\sigma_m}\tau_d-\left[A_{\nu,m}I_{\mu_m+1}(\sigma_m\gamma_{m-1})-B_{\nu,m}K_{\mu_m+1}(\sigma_m\gamma_{m-1})\right]\right.\\ &\frac{\gamma_{m-1}^{\mu_m+1}}{\sigma_m}\tau_d+\sum_{n=1}^{\infty}\frac{\hat{g}_n}{\hat{\omega}_{m,n}}\left[\left(\hat{A}_{m,n}J_{\mu_m+1}\left(\hat{\omega}_{m,n}\gamma_m\right)+\hat{B}_{m,n}Y_{\mu_m+1}\left(\hat{\omega}_{m,n}\gamma_m\right)\right)\gamma_m^{\mu_m+1}-\left(\hat{A}_{m,n}J_{\mu_m+1}\left(\hat{\omega}_{m,n}\gamma_{m-1}\right)+\hat{B}_{m,n}Y_{\mu_m+1}\left(\hat{\omega}_{m,n}\gamma_{m-1}\right)\right)\gamma_{m-1}^{\mu_m+1}\right]\\ &\left(\frac{1-\exp\left(-\hat{\lambda}_n^2\tau_d\right)}{\hat{\lambda}_n^2}\right)+\sum_{n=1}^{\infty}\frac{\tilde{g}_n}{\tilde{\omega}_{m,n}}\left[\left(\tilde{A}_{m,n}J_{\mu_m+1}(\tilde{\omega}_{m,n}\gamma_m)+\tilde{B}_{m,n}Y_{\mu_m+1}(\tilde{\omega}_{m,n}\gamma_m)\right)\gamma_m^{\mu_m+1}-\left(\tilde{A}_{m,n}J_{\mu_m+1}(\tilde{\omega}_{m,n}\gamma_{m-1})+\tilde{B}_{m,n}Y_{\mu_m+1}(\tilde{\omega}_{m,n}\gamma_{m-1})\right)\gamma_{m-1}^{\mu_m+1}\right]\\ &\left.\left(\frac{1-\exp\left(-\tilde{\lambda}_n^2\tau\right)}{\tilde{\lambda}_n^2}\right)\right]\end{aligned} \tag{B.7}$$

$$\begin{aligned}\bar{\rho}_m(\tau)=&\frac{2}{1-\gamma_0^2}\times\\ &\left[\sum_{n=1}^{\infty}\frac{\tilde{g}_n}{\tilde{\omega}_{m,n}}\left[\left(\tilde{A}_{m,n}J_{\mu_m+1}(\tilde{\omega}_{m,n}\gamma_m)+\tilde{B}_{m,n}Y_{\mu_m+1}(\tilde{\omega}_{m,n}\gamma_m)\right)\gamma_m^{\mu_m+1}-\left(\tilde{A}_{m,n}J_{\mu_m+1}(\tilde{\omega}_{m,n}\gamma_{m-1})+\tilde{B}_{m,n}Y_{\mu_m+1}(\tilde{\omega}_{m,n}\gamma_{m-1})\right)\gamma_{m-1}^{\mu_m+1}\right]\right.\\ &\left.\exp\left(-\tilde{\lambda}_n^2\tau\right)\right]\end{aligned} \tag{B.8}$$

$$\begin{aligned}\bar{\psi}_{out}(\tau)=&\frac{2Sh_{out}}{1-\gamma_0^2}\times\\ &\left[\left[A_{\nu,M}I_{\mu_M}(\sigma_M)+B_{\nu,M}K_{\mu_M}(\sigma_M)\right]\tau_d+\sum_{n=1}^{\infty}\hat{g}_n\left[\hat{A}_{M,n}J_{\mu_M}\left(\hat{\omega}_{M,n}\right)+\hat{B}_{M,n}Y_{\mu_M}\left(\hat{\omega}_{M,n}\right)\right]\left(\frac{1-\exp\left(-\hat{\lambda}_n^2\tau_d\right)}{\hat{\lambda}_n^2}\right)\right.\\ &\left.+\sum_{n=1}^{\infty}\tilde{g}_n\left[\tilde{A}_{M,n}J_{\mu_M}(\tilde{\omega}_{M,n})+\tilde{B}_{M,n}Y_{\mu_M}(\tilde{\omega}_{M,n})\right]\left(\frac{1-\exp\left(-\tilde{\lambda}_n^2\tau_d\right)}{\tilde{\lambda}_n^2}\right)\right]\end{aligned} \tag{B.9}$$

$$\bar{\psi}_{in}(\tau)=\frac{2\gamma_0 Sh_{in}}{1-\gamma_0^2}\left[\sum_{n=1}^{\infty}\tilde{g}_n\left[\tilde{A}_{1,n}\mathrm{J}_{\mu_1}(\tilde{\omega}_{1,n}\gamma_0)+\tilde{B}_{1,n}\mathrm{Y}_{\mu_1}(\tilde{\omega}_{1,n}\gamma_0)\right]\gamma_0{}^{\mu_1}\left(\frac{1-\exp\left(-\tilde{\lambda}_n^2\tau\right)}{\tilde{\lambda}_n^2}\right)\right] \tag{B.10}$$

Supplementary material

Supplementary material associated with this article can be found, in the online version, at doi:10.1016/j.ijheatmasstransfer.2022.122572.

References

[1] R.V. Jeger, et al., Drug-coated balloons for coronary artery disease: third report of the international DCB consensus group, JACC 13 (2020) 1391–1402, doi:10.1016/j.jcin.2020.02.043.

[2] G.G. Stefanini, D.R. Holmes, Drug-eluting coronary artery stents, N. Engl. J. Med. 368 (2013) 254–265, doi:10.1056/NEJMra1210816.

[3] I. Rykowska, I. Nowak, R. Nowak, Drug-eluting stents and balloons—materials, structure designs, and coating techniques: a review, Molecules 25 (2020) 4624, doi:10.3390/molecules25204624.

[4] R. Iyer, A.E. Kuriakose, S. Yaman, L.-C. Su, D. Shan, J. Yang, et al., Nanoparticle eluting-angioplasty balloons to treat cardiovascular diseases, Int. J. Pharamceut. 554 (2019) 212–223, doi:10.1016/j.ijpharm.2018.11.011.

[5] S. McGinty, A decade of modelling drug release from arterial stents, Math. Biosci. 257 (2014) 80–90, doi:10.1016/j.mbs.2014.06.016.

[6] K. Kolandaivelu, C.C. O'Brien, T. Shazly, E.R. Edelman, V.B. Kolachalama, Enhancing physiologic simulations using supervised learning on coarse mesh solutions, J. Royal Soc. Interface 12 (2015) 1–10, doi:10.1098/rsif.2014.1073.

[7] V.B. Kolachalama, S.D. Pacetti, J.W. Franses, J.J. Stankus, H.Q. Zhao, T. Shazly, et al., Mechanisms of tissue uptake and retention in zotarolimus-coated balloon therapy, Circulation 127 (2013) 2047–2055, doi:10.1161/CIRCULATIONAHA.113.002051.

[8] Sarifuddin, P.K. Mandal, Effect of interstitial fluid flow on drug-coated balloon delivery in a patient-specific arterial vessel with heterogeneous tissue composition: a simulation study, Cardiovasc. Eng. Technol. 9 (2018) 251–267, doi:10.1007/s13239-018-0345-2.

[9] K. Anbalakan, H.W. Toh, H.Y. Ang, M.L. Buist, H.L. Leo, Assessing the influence of atherosclerosis on drug coated balloon therapy using computational modelling, Eur. J. Pharm. Biopharm. 158 (2021) 72–82, doi:10.1016/j.ejpb.2020.09.016.

[10] A.R. Tzafriri, S.A. Parikh, E.R. Edelman, Taking paclitaxel coated balloons to a higher level: predicting coating dissolution kinetics, tissue retention and dosing dynamics, J. Control. Release 310 (2019) 94–10, doi:10.1016/j.jconrel.2019.08.019.

[11] M. Colombo, A. Corti, S. Berceli, F. Migliavacca, S. McGinty, C. Chiastra, 3D modelling of drug-coated balloons for the treatment of calcified superficial femoral arteries, PLoS ONE 16 (2021) e0256783, doi:10.1371/journal.pone.0256783.

[12] S. McGinty, G. Pontrelli, On the role of specific drug binding in modelling arterial eluting stents, J. Math. Chem. 54 (2016) 967–976, doi:10.1007/s10910-016-0618-7.

[13] G. Pontrelli, F. de Monte, Modeling of mass dynamics in arterial drug-eluting stents, J. Porous Media 12 (2009) 19–28, doi:10.1615/JPorMedia.v12.i1.20.

[14] G. Pontrelli, F. de Monte, Mass diffusion through two-layer porous media: an application to the drug-eluting stent, Int. J. Heat Mass Transf. 50 (2007) 3658–3669, doi:10.1016/j.ijheatmasstransfer.2006.11.003.

[15] G. Pontrelli, F. de Monte, A multi-layer porous wall model for coronary drug-eluting stents, Int. J. Heat Mass Transf. 53 (2010) 3629–3637, doi:10.1016/j.ijheatmasstransfer.2010.03.031.

[16] J. Escuer, I. Aznar, C. McCormick, E. Peña, S. McGinty, M.A. Martínez, Influence of vessel curvature and plaque composition on drug transport in the arterial wall following drug-eluting stent implantation, Biomech. Model. Mechanobiol. 20 (2021) 767–786, doi:10.1007/s10237-020-01415-3.

[17] M. d'Errico, P. Sammarco, G. Vairo, Analytical modeling of drug dynamics induced by eluting stents in the coronary multi-layered curved domain, Math. Biosci. 267 (2015) 79–96, doi:10.1016/j.mbs.2015.06.016.

[18] A. Jain, L. Zhou, M. Parhizi, Multilayer one-dimensional convection-diffusion-reaction (CDR) problem: analytical solution and imaginary eigenvalue analysis, Int. J. Heat Mass Transf. 177 (2021) 121465, doi:10.1016/j.ijheatmasstransfer.2021.121465.

[19] S. McGinty, S. McKee, R. Wadsworth, C. McCormick, Modeling arterial wall drug concentrations following the insertion of a drug-eluting stent, SIAM J. Appl. Math. 73 (2013) 2004–2028, doi:10.1137/12089065X.

[20] C.A. Kennedy, M.H. Carpenter, Additive Runge-Kutta schemes for convection-diffusion-reaction equations, Appl. Numer. Math. 44 (2003) 139–181, doi:10.1016/S0168-9274(02)00138-1.

[21] V. Joshi, R. Jaiman, A positivity preserving variational method for multi-dimensional convection–diffusion–reaction equation, J. Comput. Phys. 339 (2017) 247–284, doi:10.1016/j.jcp.2017.03.005.

[22] A. Tzafriri, A. Groothuis, G. Price, E. Edelman, Stent elution rate determines drug deposition and receptor-mediated effects, J. Control. Release 161 (2012) 918–926, doi:10.1016/j.jconrel.2012.05.039.

[23] A. Tzafriri, A. Levin, E. Edelman, Diffusion-limited binding explains binary dose response for local arterial and tumour drug delivery, Cell Proliferat. 42 (2009) 348–363, doi:10.1111/j.1365-2184.2009.00602.x.

[24] R. Chiba, An analytical solution for transient heat conduction in a composite slab with time-dependent heat transfer coefficient, Math. Probl. Eng. 2018 (2018) 4707860, doi:10.1155/2018/4707860.

[25] M. Abramowitz, I. Stegun (Eds.), Handbook of Mathematical Functions With Formulas, Graphs, and Mathematical Tables, Dover Publications, Mineola, NY, 1974 ISBN 978-0-486-61272-0.

[26] F. Bozsak, J.-M. Chomaz, A.I. Barakat, Modeling the transport of drugs eluted from stents: physical phenomena driving drug distribution in the arterial wall, Biomech. Model. Mechanobiol. 13 (2014) 327–347, doi:10.1007/s10237-013-0546-4.

[27] D. Anthony, D. Sarkar, A. Jain, Non-invasive, transient determination of the core temperature of a heat-generating solid body, Sci. Rep. 6 (2016) 35886 1-10, doi:10.1038/srep35886.